THE ASTROPHYSICAL JOURNAL, 212:832–858, 1977 March 15

STARS WITH DEGENERATE NEUTRON CORES. I. STRUCTURE OF EQUILIBRIUM MODELS*

KIP S. THORNE
W. K. Kellogg Radiation Laboratory, California Institute of Technology
AND
ANNA N. ŻYTKOW
W. K. Kellogg Radiation Laboratory, California Institute of Technology; and
Institute of Astronomy, Polish Academy of Sciences, Warsaw, Poland
Received 1976 May 26

ABSTRACT

Stars with massive envelopes ($M_{\rm env} \gtrsim 1\ M_\odot$) and degenerate neutron cores ($M_{\rm core} \sim 1\ M_\odot$, $R_{\rm core} \sim 10$ km) are analyzed theoretically: General-relativistic equations of structure are derived under the assumptions of hydrostatic and thermal equilibrium, spherical symmetry, no rotation, and no magnetic field. Numerical models are constructed, and analytic expressions are derived for the stellar structure in various interior regions. It is argued that all nonrotating, equilibrium models probably resemble qualitatively those constructed in this paper. Brief discussions are given of the stability and evolution of the models, and of prospects for identifying such stars observationally.

Viewed externally, our models are extreme M supergiants ($L \sim 3 \times 10^4$ to $1.3 \times 10^5\ L_\odot$, $T_{\rm photosphere} \sim 2600$ to 3100 K, $R_{\rm photosphere} \simeq 1000\ R_\odot$). The large, diffuse envelope of each model is separated from its compact core by a thin ($\sim$40 meter) energy-generation layer called the "halo." The envelope convects from the outer edge of the halo all the way out to the photosphere. Matter contracts from the envelope through the halo and into the core at a rate of $\sim 1 \times 10^{-8}\ M_\odot\ {\rm yr}^{-1}$. The contracting matter releases its gravitational energy and burns its hydrogen and helium while passing through the halo. When the envelope mass exceeds $\sim 10\ M_\odot$, the hydrogen-burning shell occurs at the halo-envelope interface, and the products of hot ($T \approx 1 \times 10^9$ K) non-equilibrium hydrogen burning are convected directly from the burning shell out to the photosphere, where they should be observable.

Subject headings: relativity — stars: interiors — stars: late-type — stars: neutron — stars: supergiants

I. INTRODUCTION AND OVERVIEW

a) Stars with Neutron Cores Compared with Stars with White-Dwarf Cores

This is the first of several papers devoted to the question, What are the possible equilibrium states for a star consisting of a massive nondegenerate envelope surrounding a degenerate neutron core?

The analogous question, What are the equilibrium states for a star with a massive, nondegenerate envelope surrounding a degenerate-electron (white-dwarf) core? has a well-known answer: Such stars are red giants which reside near the Hayashi track of the H-R diagram. In these stars matter continually, but slowly, flows from the inner regions of the envelope onto the outer regions of the core, passing through one or more nuclear-burning shells as it flows. The inflow releases nuclear and gravitational energy, converting it into stellar luminosity L:

$$L = L_{\rm nuc} + L_{\rm grav}\,, \qquad L_{\rm nuc} = \dot{M}c^2 Q\,, \qquad L_{\rm grav} = \dot{M}c^2 \frac{GM_c}{R_c c^2}\,; \tag{1.1a}$$

$$Q \approx 0.007\,, \qquad GM_c/R_c c^2 \approx 10^{-4}. \tag{1.1b}$$

(Here $\dot{M}$ is the rate of mass flow into the core, Q is the efficiency of nuclear burning for converting rest mass into thermal energy, and $GM_c/R_c c^2$ is the analogous efficiency of gravitational contraction with M_c and R_c the core mass and radius.)

For the case of a star with neutron core, one might expect a similar answer: Red-giant star near the Hayashi track; gradual inflow of matter from envelope to core; formula (1.1a) for energy generation again valid, but now with

$$Q \approx 0.007\,, \qquad GM_c/R_c c^2 \approx 0.15\,. \tag{1.1b′}$$

* Supported in part by the National Science Foundation [AST 75-01398 A01].

The enormous strengthening of the gravitational potential, GM_c/R_c, when the white-dwarf core is replaced by a neutron core, has two consequences: (i) The relative roles of nuclear burning and gravitation as sources of luminosity are reversed:

$$L_{\rm nuc}/L \approx 0.99\,,\ L_{\rm grav}/L \approx 0.01 \quad \text{for white-dwarf core;} \tag{1.2a}$$

$$L_{\rm nuc}/L \approx 0.04\,,\ L_{\rm grav}/L \approx 0.96 \quad \text{for neutron core.} \tag{1.2b}$$

(ii) The time scale for marked evolution of the star is much longer in the neutron case than in the white-dwarf case, if one compares stars of similar luminosities:

$$\frac{\tau_{\rm neut}}{\tau_{\rm w.d.}} \approx \frac{1\ M_\odot/\dot{M}_{\rm neut}}{1\ M_\odot/\dot{M}_{\rm w.d.}} \approx \frac{L_{\rm w.d.}/0.007\ c^2}{L_{\rm neut}/0.15\ c^2} = 20\,\frac{L_{\rm w.d.}}{L_{\rm neut}} \gg 1\,. \tag{1.3}$$

b) Qualitative Overview of the Internal Structure

The above discussion is corroborated by the detailed stellar models that we shall construct in this paper—so long as the total mass of the star is $\lesssim 10\ M_\odot$ (we shall call such stars "giants"). For $M \gtrsim 10\ M_\odot$ ("supergiants") our models have convective envelopes that extend all the way into the hydrogen-burning shell. As a consequence, most of the burned material is recycled back into the envelope, rather than being passed on into the core; the relative importance of nuclear and gravitational energy generation is reversed back to the white-dwarf-type situation, $L_{\rm nuc} \gg L_{\rm grav}$; the evolution of the star is dominated by chemical changes in the envelope rather than by growth of the core; and the evolution time scale is comparable to the white-dwarf-core case.

Except for location of the hydrogen-burning shell and its resulting influence on the star's evolution (giant versus supergiant), our stellar models all have similar structures. Figure 1 depicts their common structure, and defines a number of terms ("envelope," "knee," "halo," "core," ...) which we shall use throughout this paper in discussing our models.

The stellar structure depicted in Figure 1 is very peculiar; many of its features are unique to stars with neutron cores, and violate intuition based on studies of more normal stellar models. For example: (i) In no other type of stellar model yet constructed does a single convection zone link the photosphere to a nuclear-burning region. (ii) The region between the core and the base of the convective envelope is nearly isothermal and has a total thickness of only ~ 40 meters; we call this region the star's "halo." (iii) All of the gravitational energy release occurs in the upper regions ($\lesssim 20$ meters) of this halo. (iv) In giant models this halo contains both the hydrogen- and helium-burning shell sources, each with thickness $\lesssim 5$ meters; in supergiants the hydrogen-burning shell overlaps the envelope, so the halo contains only the helium-burning shell.

c) Observable Features of the Models

Unfortunately all of these extreme halo conditions are thoroughly hidden from the prying eyes of the astronomer by the huge, tenuous, red-giant envelope. The envelope acts as a buffer: Consider two stellar models with the same core mass, envelope mass, and total luminosity, but with different cores (white-dwarf versus neutron). Imagine comparing these models by swimming outward from the core through the envelope to the photosphere. The differences one would see are enormous near the core; but they would gradually die away as one moves outward through the envelope. At the photosphere only one tiny difference would remain: the star with a neutron core would be slightly redder, by $\Delta \log T_{\rm ph} \ll 0.1$.

Put differently: aside from chemical composition (see below), the only distinguishing external feature of our models with neutron cores is their extreme redness: because they sit precisely on the edge of the Hayashi forbidden region, they must be the reddest stars in the universe; but they will be redder than stars at the tip of the normal giant branch by only a very slight amount, $\Delta \log T_{\rm ph} < 0.1$. This difference is so slight that it will get lost in other effects (reddening by circumstellar material and interstellar material, differences in chemical composition causing differences in $T_{\rm ph}$, uncertainties in values of molecular opacities and convective mixing lengths, etc.). Hence, this redness difference is not a good "handle" to use in observational searches for stars with neutron cores.

Thus far our model building has yielded only one good observational handle—and we are not yet sure of its details: In our supergiant models convection should carry the products of hydrogen burning directly from the nuclear-burning shell to the photosphere. The hydrogen will be burned by a hot ($T \approx 1 \times 10^9$ K), nonequilibrium CNO–Ne reaction network, and presumably will produce very peculiar relative abundances of various catalyst isotopes (^{18}O, ^{17}O, ^{16}O, ^{13}C, ^{12}C, etc.). It may be possible to measure these abundances in the photosphere by observational studies of molecular band spectra—e.g., rotational bands of carbon monoxide, vanadium oxide, and titanium oxide. In collaboration with Michael Newman we are now calculating the details of the nuclear reaction chains and the resulting abundances; we shall publish them in a subsequent paper in this series.

It is conceivable that our models may experience instabilities that do not occur in white-dwarf-cored stars with massive envelopes—and that the effects of these instabilities might be discernible observationally. However, we have not yet undertaken detailed stability analyses of our models.

Our preliminary, crude studies of stability suggest that the envelopes of our models might be unstable against complete disruption for $M \lesssim 3\ M_\odot$ when $M_{\rm core} \approx 1\ M_\odot$. However, it seems quite possible that our stars are stable against disruption if $M \gtrsim 5\ M_\odot$, and in this case live for 10^7 to 10^8 years.

Although a red giant of given luminosity may live 20 times longer if it has a neutron core than if it has a white-dwarf core, giants with neutron cores may well be much less abundant in the universe than giants with white-dwarf cores: When massive stars form neutron cores by gravitational collapse, their loosely bound, tenuous envelopes probably get ejected. If so, then the only way the neutron core can become a red giant is by acquiring a new envelope—and the only place this is likely to happen is in a very close binary system, by supercritical mass transfer from a companion or by a cannibalistic sinking into the companion's center and eating of the companion's core. Recently Ostriker and Paczynski (1975) have speculated about such events.

d) Previous Work on Stars with Neutron Cores

We are aware of the following previous work on stars with neutron cores: (i) In the 1930s a number of people speculated about the structures and stellar-evolutionary roles of such stars, but no detailed analyses were carried out and no firm conclusions were reached; see, e.g., Gamow (1937), Landau (1937), Oppenheimer and Volkoff (1939). For example, Landau (1937) noticed the enormous efficiency, $GM_c/R_c c^2 \approx 0.15$, with which contraction onto a neutron core can liberate energy; he proposed that this might be the source of the luminosity of the Sun and other stars; and he suggested that one try to build stellar models of this type. (Presumably nobody tried because shortly thereafter nuclear burning was recognized as the true energy source.) (ii) Murray Gell-Mann tells us that in the early 1950s Enrico Fermi speculated that stars with neutron cores would be red supergiants; however, so far as we have been able to learn, Fermi never published anything on this subject. (iii) Zel'dovich, Ivanova, and Nadyozhin (1972) studied the contraction of small-mass envelopes ($M_{\rm env} \lesssim 10^{-5}\ M_\odot$) onto neutron stars. They found a neutrino luminosity far greater than the photon luminosity; and they speculated that, by analogy, stars with neutron cores and massive envelopes might be unstable against collapse of the envelope onto the core, with the collapse energy being carried off by neutrinos. We shall argue later (§ VI below) that our models do not suffer this "neutrino-runaway instability." (iv) Stothers and Cheng (1974) speculated that the envelope of a star with a neutron core would be rapidly ejected by a secular instability. Our studies (§ VI below) suggest that this might be correct for low-mass envelopes ($M_{\rm env} \lesssim 2\ M_\odot$), but that more massive envelopes might be stable against disruption. (iv) Paczynski (private communication, 1973) suggested that one of us (A. N. Ż.) try to construct stellar models with neutron cores, and we decided to collaborate on the project. We published a brief account of our results as Thorne and Żytkow (1975). (v) Ostriker and Paczynski (1975) speculated on the role of such stars in the evolution of close binary systems (see above).

In the last section of this paper we shall list a number of further investigations that are needed.

e) Notation Used in This Paper

We here summarize for future reference those mathematical symbols which are used in more than one place in this paper, and we give reference to equations which contain further details. Equation numbers beginning with T are from Thorne (1977); those beginning with A are in the appendix of this paper. We list first the "main symbols" and then the "subscripts and superscripts."

MAIN SYMBOLS:

a	radiation constant appearing in $P_{\rm rad} = \frac{1}{3}aT^4$.
B	nuclear binding energy per unit rest mass; eqs. (T, 5b) and (2.23).
c	speed of light.
C	abundance of carbon (^{12}C) by mass.
$\mathscr{E}$	relativistic energy correction factor; eq. (T, 6d).
$F_{\rm conv}$	energy flux carried convectively; eq. (T, 10).
g	local acceleration of gravity; eq. (T, 8a).
G	Newton's gravitation constant.
$G(T)$	Sampson's Klein-Nishina correction factor for electron-scattering opacity; eq. (2.32c).
$\mathscr{G}$	relativistic gravitational-acceleration correction factor; eq. (T, 6c).
H	scale height [H_P eq. (T, 8b); H_{Pg} eq. (4.5); H_h eq. (4.20b)].
$\mathscr{H}$	relativistic enthalpy correction factor; eq. (T, 6e) [$\mathscr{H}_g$ eq. (4.2)].
k	Boltzmann constant.
l_t	mixing length; eq. (T, 8c).
L	total nonneutrino luminosity as measured at photosphere and by observers far from star; eq. (4.8b) [$L_{\rm grav}$ eq. (4.8a)].
L_r	nonneutrino luminosity as measured at radius r inside star; eqs. (T, 4a) and (2.43) [$L_r^{\rm nuc}$ eq. (4.16); $L_r^{\rm crit}$ eq. (4.4b); $L_r^{\rm rad}$ eq. (4.3)].
L^ν	total neutrino luminosity as measured at photosphere [$L^{o\nu}$ eq. (T, 13); $L^{n\nu}$ eq. (T, 13)].

L_r^{ν}	total neutrino luminosity as measured at radius r [L_r^{ov} eq. (T, 4c); L_r^{nv} eqs. (T, 4b) and (2.42a)].
$m_{\rm H}$	mass of hydrogen atom.
M	total rest mass; eq. (T, 13) [M_r eq. (T, 2a)].
M_t	total mass-energy; eq. (T, 13) [$M_{\rm tr}$ eq. (T, 3b)].
$\dot{M}$	rate of inflow of rest mass from envelope to core; eqs. (2.14) and (2.44).
P	pressure; eq. (T, 5a).
r and R	radius; equal to $(1/2\pi) \times$ (circumference); eqs. (T, 3a) and (T, 13).
$\mathscr{R}$	relativistic redshift correction factor; eq. (T, 6a) and (2.36) [$\mathscr{R}_c$ eq. (2.42b); $\mathscr{R}_{\rm H}$ eq. (2.42b)].
t	Schwarzschild coordinate time; eq. (T, 2b).
T	temperature; eq. (T, 1b); $T_9 \equiv T/10^9$ K; $T_k \equiv kT/1$ keV.
v	locally measured velocity [inflow velocity $v_{\rm in}$ eq. (2.19); turbulent velocity v_t eq. (T, 10c)].
X	abundance of hydrogen (^{1}H) by mass.
X_i	abundance of nuclear species i by mass; (T, 1c).
Y	abundance of helium (^{4}He) by mass.
y	electron-positron pair parameter; eq. (A.8).
Z	$1 - X - Y$; abundance of "metals" by mass.
α	luminosity parameter; eq. (2.10); except in Table 3 where α is the ratio of mixing length to pressure scale-height, $\alpha = l_t/H_p$.
α_i	nuclear reaction rate for species i; eq. (T, 5i).
β_g	P_g/P.
β_L	$1 - L_r/L_r^{\rm crit}$.
γ_g	$\beta_g/(1 - \beta_g) \equiv P_g/P_{\rm rad}$.
γ_L	$\beta_L/(1 - \beta_L) \equiv L_r^{\rm crit}/L_r - 1$.
∇	"actual gradient," $d \ln T/d \ln P$; eq. (T, 10).
$\nabla_{\rm ad}$	adiabatic gradient, eq. (T, 9b).
$\nabla_{\rm rad}$	radiative gradient; eq. (T, 9a).
ϵ	energy generation rate [$\epsilon_{\rm nuc}$ eq. (T, 5f); ϵ_{nv} eq. (T, 5g); ϵ_{ov} eq. (T, 5h)].
κ	opacity; eq. (T, 5e).
$\kappa_{\rm es}$	opacity due to scattering of photons by electrons and positrons; eq. (2.32).
$\kappa_{\rm deg.e}$	opacity against heat transport by degenerate electrons; eq. (2.31) and (2.8).
μ	mean molecular weight; eq. (4.9a) [μ_e eq. (2.30); $\mu_{\rm ion}$ eq. (2.29a)]; except in Appendix where μ is chemical potential.
Π	specific internal energy; eq. (T, 5c).
ρ	density of rest mass; eq. (T, 1a); $\rho_6 \equiv \rho/10^6$ g cm^{-3}; $\rho_{10} \equiv \rho/10^{10}$ g cm^{-3}.
σ	Stefan-Boltzmann constant; $\sigma = ac/4$.
τ	optical depth measured from the star's surface inward.
Φ	gravitational potential; eqs. (T, 3c) and (2.34).

SUBSCRIPTS AND SUPERSCRIPTS:

c	outer edge of core (point where electron degeneracy sets in; $\rho \approx 10^6$ g cm^{-3}).
C	carbon; or at the center of the carbon-burning shell (point where C = 0.5).
CC	^{12}C + ^{12}C reaction network.
CNO	CNO reaction network for hydrogen burning.
crit	critical luminosity.
e	ionization electrons.
env	envelope of star.
g	gas (plasma; everything except radiation).
grav	gravitational.
h	halo of star.
H	hydrogen; or at the center of the hydrogen-burning shell (point outside which half the nuclear energy release has occurred).
He	helium; or at the center of the helium-burning shell (point where $Y = 0.5$).
i	nuclear species i.
in	mass inflow from envelope to core.
ion	ions.
K	knee of star.
m–i	at the interface between the middle and inner regions; eq. (2.2).
nuc	nonneutrino energy from nuclear burning.
nv	neutrino energy from nuclear burning; eq. (T, 4b).
ov	neutrino energy from processes other than nuclear-burning networks; eq. (T, 4c).
o–m	at the interface between the outer and middle regions; eq. (2.1).

P	pressure.
pair	electron-positron pairs.
ph	photosphere of star.
r	measured at radius r.
rad	radiation.
s	sound.
t	turbulence (convective motion); except in M_t and M_{tr} where t means "total."
3α	3α reaction network for helium burning.
$-$	electrons (including ionization electrons and pair electrons).
$+$	positrons.

f) Outline of Paper

In § II we lay down the physical and mathematical foundations for the construction of models of stars with neutron cores. Section III is a series of graphs and tables displaying the details of our numerical models. In § IV we discuss and analyze analytically our "giant models"; and in § V we do the same for our "supergiants." In §§ VI and VII we discuss briefly the stability and evolution of our models. Finally, § VIII is a list of topics which need further investigation.

II. FOUNDATIONS FOR OUR MODEL BUILDING

In this section we describe the assumptions, equations, and numerical techniques that underlie our computer-generated models and underlie our analytic approximations to them.

We begin by demanding that our models be spherically symmetric, nonrotating, and devoid of magnetic fields, and that they be in slowly evolving equilibrium states (evolution time scale long compared to hydrodynamic and thermal time scales).

Because of the strength of gravity near the neutron core, we ask that our models be general-relativistic rather than Newtonian—except that Newtonian analyses suffice in the outer region of the star and in order-of-magnitude estimates of effects.

a) Partition of Model into Three Regions

In our computer calculations we divide each model into three regions (see Fig. 1). The "*outer region*" contains the atmosphere, the photosphere, and the static part of the envelope—i.e., that portion of the envelope in which mass inflow has negligible effects. The "*middle region*" contains the inflowing part of the envelope, the halo, and the outermost layers of the core where the carbon-burning shell is located. The "*inner region*" is the entire core, except its outermost layers.

The boundary between outer and middle regions, r_{o-m}, occurs where the inflow first begins to influence the local luminosity L_r; this happens when the enthalpy $\Pi + p/\rho$ and/or the gravitational potential GM_{tr}/r becomes larger than ~ 0.003 of its maximum value ($\sim 0.1\ c^2$). Thus, we arbitrarily set

$$r_{o-m} = \left(\text{that radius at which } \frac{\Pi}{c^2} + \frac{P}{\rho c^2} + \frac{GM_{tr}}{c^2 r} = 3 \times 10^{-4}\right) . \tag{2.1}$$

(All symbols used here are explained in § I*e*.)

The boundary between the middle and inner regions, r_{m-i}, occurs where nuclear energy generation is no longer significant. In our models more than 99% of all energy generation is by gravity and by thermonuclear hydrogen burning, so it is not very necessary to include the effects of helium, carbon, or further nuclear-burning stages. However, to see what their effects may be, we have included helium burning and carbon burning. It turns out that the carbon burning is complete by a density of $\rho \approx 1 \times 10^8$ g cm^{-3}. Therefore, we choose

$$r_{m-i} = (\text{that radius at which } \rho = 3 \times 10^8 \text{ g cm}^{-3}) . \tag{2.2}$$

b) Structure of the Inner Region

In the inner region the high density enforces degeneracy and thereby guarantees that the hydrostatic structure (ρ, P, r, M_{tr}, Φ as functions of M_r) is decoupled from the thermal structure (L_r and T as functions of M_r).

The massive envelope of the star can influence the hydrostatic structure of the inner region in only one way: by its weight, which squeezes the inner region to a pressure and density, at given M_r, that are higher than for a bare (envelope-free) neutron star. This compressional effect can be evaluated by integrating the equation of hydrostatic equilibrium outward through the star (throughout this subsection we use Newtonian theory because 50% accuracy is adequate):

$$P(M_r) = \int_{M_r}^{M} -\frac{dP}{dM_r}\, dM_r = \int_{M_r}^{M} \frac{GM_r}{4\pi r^4}\, dM_r . \tag{2.3}$$

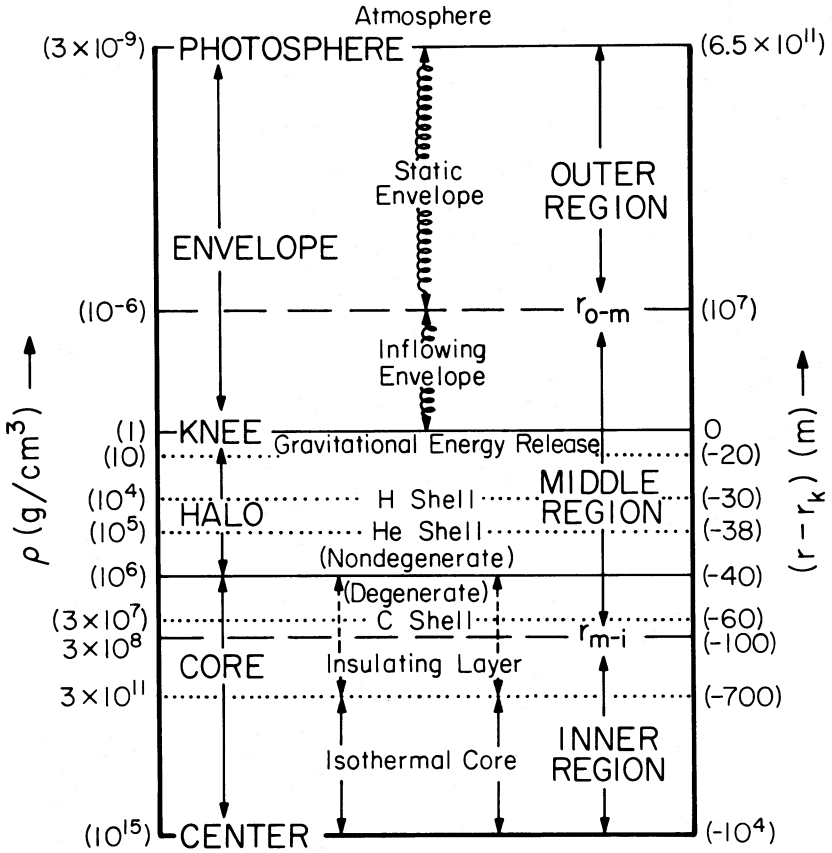

FIG. 1.—The structure of stars with degenerate neutron cores. The interior of the box lists a number of features of the stellar interior. The locations of those features are indicated on the left of the box in terms of density ρ, and on the right of the box in terms of radius minus the radius of the star's "knee," $r - r_K$. Numbers not in parentheses are exact and apply to all of our models. Numbers in parentheses are taken from a general-relativistic "giant" model (Table 1) with total mass $M_t = 5\ M_\odot$, total core mass $M_{tc} = 1\ M_\odot$, and core radius $R_c = 10$ km—but these parenthesized numbers are qualitatively correct for all models.

In the left column of the box are listed the major regions of the stellar interior: the *photosphere*, which is the point with optical depth $\tau = \frac{2}{3}$; the *envelope*, which extends downward from the photosphere to the knee; the *knee*, which is the point where envelope convection stops; the *halo*, which extends inward from the knee to the point of onset of electron degeneracy; and the *core*, which extends from the onset of electron degeneracy in to the *center* of the star.

In the middle column of the box are listed a number of subregions of the stellar interior including: the *atmosphere*, which lies above the photosphere; the *static envelope*, which is a convective region extending from the photosphere down to a (arbitrarily chosen) radius r_{o-m} where inflow of matter from envelope to core becomes important; the *inflowing envelope*, which is also convective and extends downward from r_{o-m} to the star's knee where convection ceases; the *region of gravitational-energy release*, which extends inward from the knee to a density $\rho \sim 10\rho_{\rm knee}$; the *hydrogen-burning shell*, *helium-burning shell*, and *carbon-burning shell*; an *insulating layer* which extends from the onset of electron degeneracy down to the point $\rho = 3 \times 10^{11}$ g cm^{-3} where neutrons drip off the atomic nuclei to form a superconducting, superfluid medium; and the *isothermal core* in which $T|g_{00}|^{1/2} \equiv T\mathscr{R}$ is nearly constant, and which extends from $\rho = 3 \times 10^{11}$ in to the center of the star.

In the right column are listed three regions into which we subdivide the model for computational purposes: the *outer region*, which includes atmosphere, photosphere, and static envelope; the *middle region*, which includes contracting envelope, halo, and the outermost part of the core (down to radius r_{m-i} where $\rho = 3 \times 10^8$ g cm^{-3}); and the *inner region*, which includes the remainder of the core.

Supergiant models ($M \gtrsim 10\ M_\odot$) differ from giant models ($M \lesssim 10\ M_\odot$; depicted in this figure) in only one qualitative way: the hydrogen-burning shell overlaps the knee and envelope instead of being confined to the halo.

The fractional contribution of the nondegenerate envelope and halo (region with $\rho \lesssim 10^6$) to the inner-region pressure is

$$\frac{(\Delta P)_{\rm env}}{P} = \frac{1}{P}\int_{10^6}^{0} \frac{GM_r}{4\pi r^4}\frac{dM_r}{d\rho}\,d\rho\,. \tag{2.4}$$

The amount of envelope and halo matter below $r = 2 \times 10^4$ km turns out to be $\lesssim 10^{-10}\ M_\odot$ (see Tables 1 and 2), which is far less than the amount of core matter between $\rho = 1 \times 10^8$ and $\rho = 3 \times 10^8$ g cm^{-3}; hence, in evaluating

expression (2.4) we can ignore the envelope matter at $r < 2 \times 10^4$ km—i.e., we can regard the envelope as a mass $M \lesssim 10\ M_\odot$ residing at $r > 2 \times 10^4$ km:

$$\frac{(\Delta P)_{\rm env}}{P} \lesssim \frac{1}{P}\frac{G(10\ M_\odot)^2}{4\pi(2\times 10^4\ {\rm km})^4} \approx \frac{1\times 10^{23}\ {\rm dyn\ cm^{-2}}}{P} \lesssim \frac{1\times 10^{23}}{P_{m\text{-}i}} \simeq \frac{1\times 10^{23}}{1\times 10^{26}} \ll 1\,. \tag{2.5}$$

This result allows us to conclude that the envelope has no significant influence on the hydrostatic structure of the inner region; the inner region will have the same hydrostatic structure as a bare (envelope-free) neutron star.

Turn next to the thermal structure of the inner region. At densities above $\rho = 3 \times 10^{11}$ ("neutron-drip point") the heat conductivity is so high that the star is very nearly isothermal [$T \approx$ const. in Newtonian theory; $T\mathscr{R} \approx$ const. in general relativity]. Almost all of the core mass is contained in this isothermal region of the core. Between this isothermal core and the halo ($3 \times 10^{11} \gtrsim \rho \gtrsim 10^6$) is a thin "insulating layer" of degenerate-electron matter which thermally isolates the core from the rest of the star. We have arbitrarily placed our middle-inner region dividing line $r_{m\text{-}i}$ in the center of the insulating layer, at $\rho = 3 \times 10^8$.

Let us estimate the maximum heat flow that the insulating layer can support. For ease of computation we shall confine attention to the region in which the electrons are fully relativistic, $10^7 < \rho < 3 \times 10^{11}$—i.e., we shall ignore the outermost part of the insulating layer, $10^6 \lesssim \rho < 10^7$. Our estimate relies on the following equation, which is a combination of the (relativistic) equation of diffusive heat transfer (eqs. [2.20h] and [T, 9a]) and the relativistic-degenerate-electron equation of state $P = (4.89 \times 10^{14}\ {\rm dyn\ cm^{-2}})(\rho/g\ {\rm cm^{-3}})^{4/3}$:

$$\frac{d\ln T}{d\ln \rho} = \frac{\kappa}{12\pi}\frac{L_r\mathscr{R}_c}{GcM_{tr}}\frac{P}{P_{\rm rad}} = 108\,\frac{\kappa}{{\rm cm^2\ g^{-1}}}\frac{{\rho_{10}}^{4/3}}{{T_9}^4}\frac{L_r}{L_\odot}\mathscr{R}_c\frac{M_\odot}{M_{tc}}\,. \tag{2.6}$$

[Here, because the insulating layer is very thin in radius and mass ($\Delta r/r \ll 1$, $\Delta M_{tr}/M_{tr} \ll 1$), the temperature redshift effect ($1 - \mathscr{E}/\mathscr{H}$ term in $\nabla_{\rm rad}$) has been ignored, and M_{tr} has been set equal to the total mass of the core M_{tc}; also the approximations $\mathscr{H} \approx 1$, $\mathscr{G} \approx M_{tr}/M_r$, and $\mathscr{V} \approx \mathscr{R}^{-1} \approx {\mathscr{R}_c}^{-1}$ have been used.] The energy transport is by electron conduction; and the dominant resistance to the conducting electrons in the relevant temperature-density regime

$$10^7 < \rho < 3\times 10^{11}\,,\quad 10^8 < T < 10^{10} \tag{2.7}$$

is electron-electron scattering above the ion-crystal melting temperature ($T_9 > T_{9\,\rm melt} \sim 1.8\ {\rho_{10}}^{1/3}$), and electron-phonon scattering below the melting temperature ($T_9 < T_{9\,\rm melt} \sim 1.8\ {\rho_{10}}^{1/3}$); see Flowers and Itoh (1975). In these two regimes the computations of Flowers and Itoh give (see their Figs. 12 and 6 for electron conductivity, which is related to opacity by $\kappa_{\rm opacity}\kappa_{\rm conductivity} = 4acT^3/3\rho$):

$$\kappa = (3.9\times 10^{-6}\ {\rm cm^2/g}){T_9}^4{\rho_{10}}^{-2} \quad \text{for } T_9 > 1.8\ {\rho_{10}}^{1/3}\,, \tag{2.8a}$$

$$\kappa = (1.11\times 10^{-5}\ {\rm cm^2/g}){T_9}^3{\rho_{10}}^{-5/3} \quad \text{for } T_9 < 1.8\ {\rho_{10}}^{1/3}\,. \tag{2.8b}$$

When inserted into equation (2.6) these opacities give

$$dT_9/d\ln\rho_{10} = 0.35\alpha T_9{\rho_{10}}^{-2/3} \text{ in molten region}\,,\quad T_9 > 1.8\ {\rho_{10}}^{1/3}\,, \tag{2.9a}$$

$$dT_9/d\ln\rho_{10} = \alpha{\rho_{10}}^{-1/3} \text{ in crystalline region}\,,\quad T_9 < 1.8\ {\rho_{10}}^{1/3}\,; \tag{2.9b}$$

$$\alpha \equiv \left(\frac{L_r}{830\,L_\odot}\right)\left(\frac{M_{tc}}{M_\odot}\right)^{-1}\mathscr{R}_c\,. \tag{2.10}$$

Equations (2.9) and (2.10) set the scale of allowable heat transfers L_r through the insulating layer: T_9 cannot change by more than a factor 3, as one traverses the insulating layer, because of the following: (i) Core neutrino losses keep the isothermal core (and thence its outer boundary, $\rho = 3 \times 10^{11}$) at a temperature $T_9 < 2$. (A neutron star cools by neutrino losses to $T_{9\,\rm core} < 6$ in 12 hours and to $T_{9\,\rm core} < 2$ in one year; see Tables 8, 9, and 10 of Tsuruta and Cameron [1966] and Fig. 1 of Tsuruta *et al.* 1972.) (ii) The outer edge of our insulating layer, $\rho = 10^7$, has $T_9 \approx 0.5$ to 1.0; see Figure 2. (iii) Neutrino losses, which vary as ${T_9}^n$ with $n \gtrsim 9/2$ in our insulating layer (Beaudet, Petrosian, and Salpeter 1967), will hold the temperature below $T_9 \approx 3$ throughout the insulating layer. These constraints on T_9, together with equations (2.9), require $|\alpha| < 1$ nearly everywhere in the degenerate electron surface layer—and, in fact, $|\alpha| \lesssim \frac{1}{8}$ in most places including our middle-inner region interface, $r = r_{m\text{-}i}$ and $\rho = 3 \times 10^8$. Hence,

$$|L_r| \lesssim (100\,L_\odot)(M_{tc}/M_\odot){\mathscr{R}_c}^{-1} \quad \text{at } \rho = 3\times 10^8\,. \tag{2.11}$$

This heat transfer is negligible compared to the star's total luminosity $L \approx 10^5\,L_\odot$.

Nuclear burning of inflowing matter will generate heat in the insulating layer of giant models at a rate

$$\left(\frac{dE}{dt}\right) \approx \begin{pmatrix}\text{total luminosity of}\\ \text{star, } \sim 5 \times 10^4\, L_\odot\end{pmatrix} \times \left(\frac{GM_{tc}}{c^2 R_c}\right)^{-1} \times \begin{pmatrix}\text{efficiency, 0.0008 of mass-to-energy}\\ \text{conversion when oxygen burns to iron}\end{pmatrix} \sim 300\, L_\odot\,. \tag{2.12}$$

Electron conductivity cannot carry away much more than $\sim 100\, L_\odot$ of this energy; the rest must be carried off by neutrinos.

The above estimates show that the inner region ($\rho > 3 \times 10^8$) is extremely well decoupled from the middle and outer regions, both hydrostatically and thermally. Its structure and thermal evolution are essentially the same as for an isolated (envelope-free) neutron star—and, thus, they are not of interest to us here. Henceforth we shall restrict attention to the middle and outer regions; and in calculating their structures we shall replace the inner region by the "insulation boundary conditions"

$$(M_r,\, M_{tr},\, \text{and } r) = \begin{pmatrix}\text{values for a "bare"}\\ \text{neutron star at } \rho = 3 \times 10^8\end{pmatrix} \quad \text{at } r = r_{m-i}\,, \tag{2.13a}$$

$$L_r = 0 \qquad \text{at } r = r_{m-i}\,. \tag{2.13b}$$

c) *The Outer Region: Physics and Computational Methods*

The outer region includes the atmosphere, the photosphere, and the static envelope; see Figure 1. Our numerical models for this region were generated using Paczynski's (1969) computer program GOB, which calculates static stellar envelopes with extended atmospheres using inward integrations that begin, in our case, at a density $\rho = 1 \times 10^{-12}$ g cm^{-3}. Each static envelope constructed by GOB can be characterized by the star's total (nonneutrino) luminosity L and mass M_t, the photospheric temperature $T_{\rm ph}$, and the envelope's nuclear abundances—assumed equal to the photospheric abundances $X_{\rm ph}$, $Y_{\rm ph}$, $Z_{\rm ph}$.

The physics and equations which go into the outer region integrations are spelled out by Paczynski (1969). In brief, the physics is this: (i) Newtonian equations of stellar structure with luminosity constant throughout and with the standard mixing-length formalism for convection; (ii) a simple gray atmosphere model based on the Eddington approximation with corrections to account for the "$1/r^2$" dilution of the outgoing radiation, which can be important in extended atmospheres; (iii) an opacity table for composition $X = 0.7$, $Z = 0.03$ (Paczynski 1970*a*), which is interpolated from the Cox-Stewart (1968) opacities and augmented by an approximation to Auman's (1967) H_2O opacity; (iv) an analytic equation of state including contributions from H_2, H, He, H^+, He^+, He^{++}, free electrons, and radiation.

d) *The Middle Region: Physics and Computational Methods*

In the middle region, which we analyze with care, general relativistic effects can be important. Therefore, our numerical computations utilized the general-relativistic equations of stellar structure—which are presented in the preceding paper (Thorne 1977; equations in this paper are denoted by a T; e.g., eq. [T, 11a]).

The middle region acts as a conduit through which mass flows from the outer region to the inner region. At any given time the total mass in this conduit is $\sim 10^{-8}\, M_\odot$ (cf. Tables 1 and 2), which is $\sim 10^8$ times less than the mass in the reservoirs (outer and inner regions) at its two ends. Assuming that the star is stable, this huge mass contrast guarantees that the rate (per unit Killing-vector-defined coordinate time t), at which rest mass flows inward across a surface of radius r, is independent of r:

$$\dot{M} \equiv (\partial M_r/\partial t)_r = \text{constant, independent of } r \text{ or } M_r\,. \tag{2.14}$$

(See Thorne 1977 and § II*e* of this paper for notation used here and below.) Also assuming the star is stable, the stellar structure is stationary on time scales $\ll 10^7$ years:

$$\left[\frac{\partial}{\partial t}\,(\text{any stellar-interior variable})\right]_{\text{fixed } r} = 0\,. \tag{2.15}$$

This stationarity, together with the identity

$$\left(\frac{\partial}{\partial t}\right)_r \equiv \left(\frac{\partial}{\partial t}\right)_{M_r} + \left(\frac{\partial M_r}{\partial t}\right)_r \left(\frac{\partial}{\partial M_r}\right)_t \tag{2.16}$$

and equation (2.14), implies a simple relationship between the time derivatives and the radial derivatives which appear in the stellar-structure equations (T, 11):

$$\left(\frac{\partial}{\partial t}\right)_{M_r} = -\dot{M}\left(\frac{\partial}{\partial M_r}\right)_t\,. \tag{2.17}$$

For example, if we let both sides of equation (2.17) act on the radius function r, and if we combine with equation (T, 11a), we obtain the relation

$$\dot{M} = 4\pi r^2 \rho v_{\rm in} \mathscr{R} , \tag{2.18}$$

where $v_{\rm in}$, the locally measured velocity of inflow of rest mass, is defined by

$$v_{\rm in} \equiv -(\mathscr{V}/\mathscr{R})(\partial r/\partial t)_{M_r} \tag{2.19}$$

(cf. eq. [T, 7]).

The above considerations are patterned after Paczynski's (1970*b*) analysis of Newtonian stars with mass inflow through stationary shell sources. When equation (2.17) is inserted into the relativistic equations of stellar structure (T, 11), it produces the relativistic analog of Paczynski's stationary-shell-source equations:

$$dr/dM_r = (4\pi r^2 \rho \mathscr{V})^{-1} , \tag{2.20a}$$

$$dM_{tr}/dM_r = \mathscr{E}/\mathscr{V} , \tag{2.20b}$$

$$d\Phi/dM_r = [GM_r/(4\pi r^4 \rho)]\mathscr{G}\mathscr{V} , \tag{2.20c}$$

$$d(L_r \mathscr{R}^2)/dM_r = \mathscr{R}^2(\epsilon_{\rm nuc} - \epsilon_{\rm ov}) + \mathscr{R}\dot{M}[d\Pi/dM_r - (P/\rho^2)d\rho/dM_r] , \tag{2.20d}$$

$$d(L_r^{\rm nv} \mathscr{R}^2)/dM_r = \mathscr{R}^2 \epsilon_{\rm nv} , \tag{2.20e}$$

$$d(L_r^{\rm ov} \mathscr{R}^2)/dM_r = \mathscr{R}^2 \epsilon_{\rm ov} , \tag{2.20f}$$

$$\begin{aligned} dX_i/dM_r &= -\mathscr{R}\alpha_i/\dot{M} \quad \text{if } \nabla_{\rm rad} \le \nabla_{\rm ad} \\ &= 0 \qquad\quad \text{if } \nabla_{\rm rad} > \nabla_{\rm ad} , \end{aligned} \tag{2.20g}$$

$$\begin{aligned} d\ln T/dM_r &= \nabla_{\rm rad} d\ln P/dM_r \quad \text{if } \nabla_{\rm rad} \le \nabla_{\rm ad} \\ &= \nabla d\ln P/dM_r \qquad \text{if } \nabla_{\rm rad} > \nabla_{\rm ad} , \end{aligned} \tag{2.20h}$$

$$dP/dM_r = -[GM_r/(4\pi r^4)]\mathscr{G}\mathscr{H}\mathscr{V} . \tag{2.20i}$$

Here we have replaced all partial derivatives $(\partial/\partial M_r)_t$ by ordinary derivatives d/dM_r because all time derivatives have disappeared from our equations. In equation (2.20g) we have imposed the physical constraint that the abundances not change radially in the convective region.

At the outer edge of the middle region the relativistic correction factors $\mathscr{E}$, $\mathscr{G}$, $\mathscr{H}$, $\mathscr{R}$, $\mathscr{V}$ all differ from unity by $\lesssim 10^{-3}$ (cf. eq. [2.1]); temperatures are so low that no nuclear burning has occurred; and consequently the above equations of structure for the middle region reduce to the standard Newtonian equations of structure with constant luminosity, which we use in our outer-region analysis. This fact guarantees that we obtain a reasonable match between middle region and outer region by simply enforcing continuity of the fundamental variables r, M_r, M_{tr}, Φ, L_r, $L_r^{\rm nv}$, $L_r^{\rm ov}$, X_i, T, and ρ at radius r_{o-m}. But in doing so we must be careful with M_r and M_{tr}: In Newtonian theory M_r is both rest mass and active gravitational mass. In general relativity M_r is rest mass, while M_{tr} is active gravitational mass; and the additive normalization of M_{tr} is crucial, while that of M_r is unimportant (all details of the model except M_r are unchanged by the renormalization $M_r \to M_r$ + constant). These facts dictate that

$$\begin{pmatrix} M_r \text{ of outer,} \\ \text{Newtonian region} \end{pmatrix} = \begin{pmatrix} M_{tr} \text{ of middle,} \\ \text{relativistic region} \end{pmatrix} \text{ at joint point } r_{o-m} ; \tag{2.21a}$$

$$\text{one need not enforce any matching condition on the middle-region } M_r . \tag{2.21b}$$

In our analysis of the middle region we use specific analytic expressions for all the auxiliary variables (pressure P, opacity κ, relativistic correction factors $\mathscr{E}$, $\mathscr{G}$, $\mathscr{H}$, $\mathscr{R}$, $\mathscr{V}$, etc.) as functions of our fundamental variables:

The nuclear species which we consider are ^{1}H (hydrogen) with abundance $X \equiv X_{\rm H}$, ^{4}He (helium) with abundance $Y \equiv X_{\rm He}$, ^{12}C (carbon) with abundance $C \equiv X_{\rm C}$, and "metals" with abundance $Z \equiv 1 - X - Y$. The binding energies per baryon relative to hydrogen are

$$\text{helium: } (1 - m_{\rm He}/4m_{\rm H})c^2 = 0.007118\, c^2 , \tag{2.22a}$$

$$\text{carbon: } (1 - m_{\rm C}/12m_{\rm H})c^2 = 0.007118(1 + 1/11.0)c^2 , \tag{2.22b}$$

$$\text{products of carbon burning: } 0.007118(1 + 1/11.0 + 1/13)c^2 ; \tag{2.22c}$$

and, consequently, the mean binding energy per baryon is

$$B = 0.007118\left[1 - X + \frac{1 - X - Y}{11.0} + \frac{1 - X - Y - C}{13}\right]c^2 . \tag{2.23}$$

In our numerical calculations we have assumed that hydrogen burns by the normal CNO cycle; this is a serious source of error, as will be discussed in § V. For the normal CNO cycle 93.6% of the energy goes into heat and 6.4% into neutrinos; hence, the energy generation rates $\epsilon_{\rm nuc}{}^{\rm CNO}$ and $\epsilon_{\nu}{}^{\rm CNO}$ are related to the rates of change of hydrogen and helium abundance $\alpha_{\rm H}{}^{\rm CNO}$ and $\alpha_{\rm He}{}^{\rm CNO}$ by

$$\epsilon_{\rm nuc}{}^{\rm CNO} = (-0.006662c^2)\alpha_{\rm H}{}^{\rm CNO} , \qquad \epsilon_{\nu}{}^{\rm CNO} = (-0.000456c^2)\alpha_{\rm H}{}^{\rm CNO} , \qquad \alpha_{\rm He}{}^{\rm CNO} = -\alpha_{\rm H}{}^{\rm CNO} . \tag{2.24}$$

The CNO energy generation rate $\epsilon_{\rm nuc}{}^{\rm CNO}$ is expressed as a function of X, Z, ρ, and T by equations (17.280), (17.282), and (17.283) of Cox and Giuli (1968) with $X_{\rm CN} \equiv Z/2$. When helium burns by the 3α process to form carbon, neutrino losses are negligible; hence

$$\epsilon_{\rm nuc}{}^{3\alpha} = (-0.000647c^2)\alpha_{\rm He}{}^{3\alpha} , \qquad \epsilon_{\nu}{}^{3\alpha} = 0 , \qquad \alpha_{\rm C}{}^{3\alpha} = -\alpha_{\rm He}{}^{3\alpha} . \tag{2.25}$$

We use equations (17.341) and (17.342) of Cox and Giuli (1968) for the 3α energy generation rate $\epsilon_{\rm nuc}{}^{3\alpha}$. We assume that carbon is burned by $^{12}{\rm C} + {}^{12}{\rm C}$ reactions, and in doing so we ignore neutrino energy generation:

$$\epsilon_{\rm nuc}{}^{\rm CC} = (-0.00055c^2)\alpha_{\rm C}{}^{\rm CC} , \qquad \epsilon_{\nu}{}^{\rm CC} = 0 . \tag{2.26}$$

We use the Arnett-Truran (1969) analytic expression for the CC burning rate together with the Salpeter–Van Horn (1969) analytic expressions for the screening factors. The non–nuclear-burning neutrino energy generation rate $\epsilon_{\rm ov}(X, Y, \rho, T)$ (including pair, photo, bremsstrahlung, and plasma neutrinos but excluding Urca) we take from Beaudet, Petrosian and Salpeter (1967).

The pressure P and specific internal energy Π are split up into four contributions: radiation, ions, ionization electrons, and pairs:

$$P = P_{\rm rad} + P_{\rm ion} + P_e + P_{\rm pair} , \qquad \Pi = \Pi_{\rm rad} + \Pi_{\rm ion} + \Pi_e + \Pi_{\rm pair} . \tag{2.27}$$

The radiation contribution has the usual form

$$P_{\rm rad} = \tfrac{1}{3}aT^4 , \qquad \Pi_{\rm rad} = 3(P_{\rm rad}/\rho) , \qquad a = 7.5647 \times 10^{-15}\ {\rm ergs\ cm^{-3}\ K^{-4}} . \tag{2.28}$$

Crystallization of the ions is ignored in P and Π; they are assumed to form a perfect gas with mean molecular weight

$$\mu_{\rm ion} = (X + Y/4 + Z/16)^{-1} , \tag{2.29a}$$

for which

$$P_{\rm ion} = (k/m_{\rm H})(\rho/\mu_{\rm ion})T , \qquad \Pi_{\rm ion} = \tfrac{3}{2}(P_{\rm ion}/\rho) . \tag{2.29b}$$

In the middle region temperatures are so high ($T \gtrsim 10^6$ K) that the plasma is fully ionized, and the mean molecular weight per ionization electron is

$$\mu_e = 2/(1 + X) . \tag{2.30}$$

Our middle region covers a temperature-density regime in which the ionization electrons range from extreme nondegeneracy to extreme degeneracy (see Fig. 2). Over the entire range we describe $P_e(T, \rho, \mu_e)$ and $\Pi_e(T, \rho, \mu_e)$ by the Eggleton-Faulkner-Flannery (1973) analytic fit to the relevant Fermi-Dirac integrals; in that fit we use their "thermodynamically consistent coefficients" (their Table 5). Near the knees of our supergiant models electron-positron pairs play a crucial role (see Fig. 2 and the discussion in § V). Fortunately, the pairs occur only in a regime $[(\rho/4 \times 10^6\ {\rm g\ cm^{-3}})^{2/3} \ll kT/m_e{}^2 \ll 1]$ where their contribution to P and Π can be expressed in fairly simple analytic form and can be added linearly onto the contributions from other sources. The relevant expressions for $P_{\rm pair}$ and $\Pi_{\rm pair}$ are given in the Appendix [eqs. (A8) and (A11)].

In the middle region all sources of opacity are negligible except electron and positron scattering of photons, and opacity to heat conduction by degenerate electrons:

$$\kappa = (1/\kappa_{\rm es} + 1/\kappa_{\rm deg.e})^{-1} . \tag{2.31}$$

We use the following analytic formula for the scattering opacity:

$$\kappa_{\rm es} = (0.4\ {\rm cm^2\ g^{-1}})\mu_e{}^{-1}(1 + 2n_+/n_e)G(T) , \tag{2.32a}$$

$$G(T) = 0.4 + 0.6 \exp(-0.04328\ T_k) , \qquad \text{if } 0 < T_k < 20 , \tag{2.32b}$$

$$G(T) = -0.13887 + 4.9871\ T_k{}^{-1/2} - 5.9479\ T_k{}^{-1} - 2.362\ T_k{}^{-3/2} , \qquad \text{if } 20 < T_k < 125 . \tag{2.32c}$$

Here $T_k = kT/(1\text{ keV}) = T/(1.160 \times 10^7\text{ K})$; $G(T)$ is the special-relativistic correction to the electron-scattering opacity; formula (2.32c) for $G(T)$ is taken from Sampson (1959); formula (2.32b) is our analytic fit to Sampson's computations; and n_+/n_e is the number density of positrons divided by the number density of ionization electrons as given by equations (A10) and (A8) of the Appendix. At the time of our numerical work the Flowers-Itoh (1975) degenerate-electron heat conductivities were not available, so we used Paczynski's (private communication) analytic fit to the tables of Canuto (1970) for carbon:

$$\log_{10}\kappa_{\text{deg.e}} = -0.05 + 0.533\,\rho_6^{-1/2} - 1.057\log_{10}\rho_6 + 2.17\log_{10}T_9\,. \tag{2.33}$$

(This formula gives a good fit for $1.05 + 3\log_{10}T_9 < \log_{10}\rho_6 < 6.15 + 3\log_{10}T_9$.) Here ρ_6 is density in units of 10^6 g cm^{-3}, and T_9 is temperature in units of 10^9 K.

Because the total amount of mass in the middle region ($\sim 10^{-8}\,M_\odot$) is negligible compared to that in the core, the gravitational field in the middle region is (very nearly) the Schwarzschild gravitational field of the core:

$$\Phi = \tfrac{1}{2}c^2\ln(1 - 2GM_{tc}/c^2r)\,. \tag{2.34}$$

Here M_{tc} is the total mass ("active gravitational mass") of the core,

$$M_{tc} \equiv M_{tr}\text{ at outer edge of core}\,. \tag{2.35}$$

In our middle-region computations we used expression (2.34) for Φ; we used the corresponding Schwarzschild-metric expressions for the redshift and volume correction factors

$$\mathscr{R} = \mathscr{V}^{-1} = (1 - 2GM_{tc}/c^2r)^{1/2}; \tag{2.36}$$

and we used expressions (T, 6c, d, e) for the relativistic correction factors $\mathscr{G}$, $\mathscr{E}$, $\mathscr{H}$.

Our computation of the radiative, adiabatic, and convective gradients ∇_{rad}, ∇_{ad}, and ∇ followed the prescription of equations (T, 9) and (T, 10) with mixing length equal to pressure scale height $l_t = H_p$. However, in our solution of the mixing equations (T, 10) we stupidly used Newtonian rather than relativistic expressions for g and H_p:

$$\begin{aligned} g &= GM_{tr}/r^2 = g_{\text{correct}}/\mathscr{V} = (0.84\text{ to }1.0)\times g_{\text{correct}} \\ H_p &= P/\rho g = (H_{p\,\text{correct}})\times\mathscr{V}\mathscr{H} = (1.00\text{ to }1.43)\times H_{p\,\text{correct}}\,. \end{aligned} \tag{2.37}$$

These errors have the same effect on the star's structure as using the correct g and H_p, but making the ratio l_t/H_p increase from its chosen value up to 1.25 its chosen value as one moves inward toward the knee of the star—i.e., they cause the convection to be a little more efficient than it should have been near the knee. Because the mixing-length theory is so unreliable, and because the convection is fairly efficient near the knee, we have not recomputed our models with these errors corrected.

e) Global Structure of the Computation

To construct a stellar model one can proceed as follows: (i) Specify the following parameters:

$$\begin{aligned} (X_{\text{ph}}, Y_{\text{ph}}, C_{\text{ph}}) &\equiv (\text{photospheric abundances of hydrogen, helium, and carbon})\,, \\ M_t &\equiv (\text{total mass of star}) \equiv (\text{"active gravitational mass"})\,, \\ M_{t,m-i} &\equiv (\text{total mass of inner region}) = M_{tc}[1 + \text{an error of } O(10^{-8})]\,. \\ R_{m-i} &\equiv (\text{radius of inner region}) = R_c[1 + \text{an error of } O(10^{-2})]\,. \end{aligned} \tag{2.38}$$

For given $M_{t,m-i}$ the value of R_{m-i} is taken from the theory of bare (envelope-free) neutron stars. (ii) Pick trial values of the quantities required for starting inward integrations:

$$L = (\text{total photon luminosity of star})\,, \tag{2.39a}$$

$$T_{\text{ph}} = (\text{photospheric temperature})\,; \tag{2.39b}$$

and also pick a trial value of

$$\dot{M} = (\text{rate of inflow of rest mass})\,, \tag{2.39c}$$

which plays an important role in the middle region but not the outer region. (iii) Integrate the equations of stellar structure inward from the photosphere to the middle–inner match point r_{m-i}; and iterate the three trial parameters L, T_{ph}, and $\dot{M}$ until the three matching conditions

$$M_{tr} = M_{t,m-i}\,,\quad r = R_{m-i}\,,\quad L_r = 0\,,\quad \text{at } \rho = 3\times 10^8\text{ g cm}^{-3} \tag{2.40}$$

(eqs. 2.13), are satisfied.

In practice the L-T_{ph}-$\dot{M}$ parameter search is not difficult: L and T_{ph} can be determined with rather good accuracy by Newtonian, outer-region integrations only (see § IV*d*)—and these can be performed once and for all, with ease, to give a family of outer-region models for subsequent join onto middle-region models. Moreover, in the case of giant stars, where negligible nuclear burning occurs in the convective region, and where—it turns out—non–nuclear-burning neutrino losses are negligible, one can express $\dot{M}$ as an analytic function of M_{tc}, R_c, and L. But in supergiants hydrogen burning in the convective envelope prevents one from finding an analytic expression for $\dot{M}$.

The principal key to the giant-star expression for $\dot{M}$ is the following equation of energy conservation, which is valid everywhere in our stellar models except in convective nuclear-burning regions:

$$L_r + L_r^{ov} + L_r^{nv} = \mathscr{R}^{-2}[\dot{M}c^2\mathscr{H}\mathscr{R} + \text{constant}]$$
$$= \dot{M}(\Pi + P/\rho - B + \Phi) + \text{constant} \qquad \text{in Newtonian limit}. \tag{2.41}$$

[This equation can be derived as follows: (i) add eqs. (2.20d, e, f); (ii) use eqs. (T, 20) and (2.17) to eliminate $\epsilon_{nuc} + \epsilon_{nv}$ (this step requires that the nuclear-burning region be nonconvective); (iii) write $-(P/\rho^2)\partial\rho/\partial M_r$ as $\partial(P/\rho)/\partial M_r - \rho^{-1}\partial P/\partial M_r$, and use eqs. (2.20i, c) and (T, 6a) to express $\partial P/\partial M_r$ in terms of $\partial\mathscr{R}/\partial M_r$; (iv) use definition (T, 6e) of $\mathscr{H}$ to bring the equation into perfect differential form; (v) integrate it.] Another key to the expression for $\dot{M}$ is a conservation law for the nuclear-burning-induced neutrino losses L_r^{nv}, again valid everywhere except in convective nuclear-burning regions:

$$L_r^{nv} = \mathscr{R}^{-2}[0.000456\,\dot{M}c^2X\mathscr{R}_H + \text{constant}]. \tag{2.42a}$$

Here $\mathscr{R}_H$ is the value of $\mathscr{R}$ at the center of the hydrogen-burning shell, which is so near the core that

$$\mathscr{R}_H = \mathscr{R}_c = (1 - 2GM_{tc}/c^2R_c)^{1/2} \tag{2.42b}$$

is a good approximation. [This equation can be derived as follows: (i) in equation (2.20e) replace ϵ_{nv} by expressions (2.24), (2.25), and (2.26), and then replace α_H^{CNO} by expression (2.20g); (ii) invoke the fact that X changes only in the hydrogen-burning shell, which is so thin that it has $\mathscr{R}$ essentially constant throughout; using this fact, write the equation in perfect differential form; (iii) integrate it.] In giant stars it turns out that the non–nuclear-burning neutrino losses are totally negligible throughout the outer and middle regions ($L^{ov} - \mathscr{R}^2L_r^{ov} \ll L_\odot$), and no significant nuclear burning occurs in convective regions. Thus, equations (2.41) and (2.42) can be combined to obtain the following relation, valid throughout the outer and middle regions:

$$L_r = \mathscr{R}^{-2}L + \mathscr{R}^{-2}\dot{M}c^2[\mathscr{H}\mathscr{R} - 1 + B_{ph}/c^2 + 0.000456\mathscr{R}_H(X_{ph} - X)]. \tag{2.43}$$

Here the constant has been evaluated at the photosphere, where $L_r = L$, $\mathscr{R}$ can be approximated as unity, $\mathscr{H} = 1 - B_{ph}/c^2$ with B_{ph} the photospheric value of the nuclear binding energy, and X_{ph} is the photospheric value of the hydrogen abundance. To obtain the desired expression for $\dot{M}$, we need only evaluate expression (2.43) at the inner edge of the carbon-burning shell, where $L_r = 0$, $X = Y = C = 0$, $\mathscr{R} = (1 - 2GM_{tc}/c^2R_c)^{1/2}$, and $\mathscr{H}$ can be approximated as $1 - B/c^2$ with B taken from equation (2.23):

$$\dot{M}c^2 = L\left[-\left(1 - \frac{2GM_{tc}}{c^2R_c}\right)^{1/2}(0.991687 + 0.000456\,X_{ph}) + 1\right.$$
$$\left. -0.007118\left(1 - X_{ph} + \frac{1 - X_{ph} - Y_{ph}}{11.0} + \frac{1 - X_{ph} - Y_{ph} - C_{ph}}{13}\right)\right]^{-1}. \tag{2.44}$$

III. NUMERICAL MODELS

Some details of our numerical models for stars with neutron cores are shown in Figure 2 and Tables 1–4. The physical features of these models will be discussed in §§ IV and V.

IV. DETAILS OF THE STELLAR STRUCTURE: GIANT MODELS

Table 1 and Figure 2 display the internal structure of a typical giant model—one with a total mass of 5 $M_\odot$ and core mass and radius of 1 $M_\odot$ and 10 km. Tables 3 and 4 show some details of other giant models. In this section we shall point out and analyze analytically some important features of these models.

a) Overall Structure

In § II*b* we explained, analytically, the hydrostatic and thermal decoupling of the core (inner region) from the rest of the star. We shall now elucidate the reasons for the gross features of the rest of the star (extremely thin halo surrounded by very deeply convective envelope).

TABLE 1

INTERNAL STRUCTURE OF A STAR WITH $M_t = 5.0\ M_\odot$, $M_{tc} = 1.0\ M_\odot$, $R_c = 10.00$ km, $X_{ph} = 0.70$, $Y_{ph} = 0.27$, $C_{ph} = 0.0$

(Note: $r_K = 10.05$ km, $M_{tK} = 1.000\ M_\odot$, $r_{m-i} = 9.95$ km. For details of notation see §I.e.)

Region	$r-r_K$ (m)	$M_{tr}-M_{tK}$ ($M_\odot$)	$\frac{2GM_{tr}}{c^2 r}$	log ρ (g/cm^3)	log T ($^\circ$K)	β_g	τ	L_r ($L_\odot$)	$L^{ov}-\mathcal{R}^2 L_r^{ov}$ ($L_\odot$)	L_r^{crit} ($L_\odot$)	∇_{ad}	∇_{rad}	∇	log v_t (cm/sec)	log v_s (cm/sec)	log v_{in} (cm/sec)
PHOTOSPHERE	6.69E11	3.94	2.18E-8	-8.739	3.423		0.667				0.0834	0.106	0.106	2.84	5.63	
	6.45E11	3.69	2.15E-8	-8.290	3.719		17.9				.386	1.63	1.63	4.43	5.87	
	6.34E11	3.57	2.13E-8	-8.413	3.942		8970.				.0869	168.	0.519	5.42	5.92	
	4.72E11	1.86	1.79E-8	-8.146	4.274						.210	298.	.534	5.54	6.25	
STATIC ENVELOPE	1.20E11	4.67E-2	2.58E-8	-7.913	4.777						.283	6.57	.496	5.89	6.60	
	3.62E9	2.32E-6	8.16E-7	-7.677	5.343						.2502	0.340	.264	6.60	7.31	
	1.72E8	9.59E-10	1.72E-5	-7.132	5.794						.2500	.2775	.2516	7.18	7.92	
							$\frac{}{1-\mathcal{R}^2 L_r/L}$									
r_{o-m}	1.67E7	4.12E-12	1.77E-4	-6.515	6.190	4.32E-3	0	41745.	<< E-20	38160.	.2500	.275	.2504	7.64	8.40	5.00
	7.65E5	9.60E-15	3.81E-3	-5.303	6.802	1.03E-3	-0.010	42306.	<< E-20	38640.	.2500	.274	.2500	8.12	9.02	6.46
	1.23E5	1.20E-15	0.0221	-4.163	7.254	6.27E-4	- .034	44127.	<< E-20	40008.	.2500	.275	.2500	8.27	9.35	6.85
INFLOWING ENVELOPE	3.38E4	4.97E-16	.0674	-3.145	7.616	5.39E-4	- .058	47348.	2.1E-20	43061.	.2500	.274	.2500	8.25	9.56	6.81
	9.61E3	2.26E-16	.150	-2.219	7.930	5.18E-4	- .073	52695.	3.5E-18	49306.	.2500	.266	.2500	8.12	9.71	6.60
	789.	2.93E-17	.273	-1.385	8.209	5.14E-4	- .078	61858.	4.0E-16	61246.	.2500	.2522	.2500	7.75	9.84	6.32
	91.7	3.62E-18	.291	-1.282	8.244	5.13E-4	- .078	63501.	7.4E-16	63449.	.2500	.2503	.2500	7.44	9.85	6.28
	29.8	1.18E-18	.293	-1.271	8.247	5.13E-4	- .078	63662.	7.8E-16	63666.	.2500	.2501	0.2500	7.28	9.85	6.28
													X	Y	C	
KNEE	0	0	.294	-1.267	8.249	5.14E-4	- .078	63741.	8.0E-16	63772.	.2500	.2500	0.700	0.270	0	6.27
	-16.2	-6.45E-19	.294	-1.248	8.250	5.34E-4	- .039	61440.	8.2E-16	63829.	.2500	.2423	.700	.270	0	6.26
Gravitational energy release	-20.5	-8.62E-19	.295	-0.954	8.250	1.05E-3	+ .456	32201.	8.2E-16	63845.	.250	.138	.700	.270	0	5.96
	-21.9	-1.01E-18	.295	-0.657	8.250	2.07E-3	.709	17201.	8.2E-16	63850.	.250	.0764	.700	.270	0	5.67
	-24.2	-1.78E-18	.295	+0.017	8.250	9.69E-3	.913	5126.	8.4E-16	63860.	.250	.0227	.700	.270	0	4.99
	-28.1	-1.72E-17	.295	1.288	8.251	0.154	.966	2025.	1.2E-15	63897.	.251	.0095	.700	.270	0	3.72
HALO	-32.0	-3.08E-16	.295	2.556	8.261	.786	.969	1836.	1.1E-14	69345.	.284	.0296	.700	.270	0	2.45
	-35.6	-3.75E-15	.295	3.576	8.336	.951	.970	1748.	2.9E-13	69090	.348	.129	.669	.301	0	1.43
H Shell	-37.0	-9.65E-15	.295	4.070	8.387	.969	.982	1049.	1.5E-12	90198.	.358	.094	.328	.642	0	0.94
	-37.5	-1.50E-14	.295	4.416	8.399	.978	.9927	434.	3.0E-12	1.18E5	.362	.041	0.026	.944	0	0.59
	-38.4	-4.06E-14	.295	4.824	8.422	.990	.9936	377.	1.2E-11	1.23E5	.371	.075	0	.970	0	0.19
	-39.8	-1.53E-13	.295	5.297	8.485	.995	.9938	365.	9.1E-11	1.33E5	.372	.141	0	.930	0.040	-0.29
He Shell	-41.0	-3.76E-13	.295	5.629	8.542	.997	.9955	265.	4.9E-10	1.48E5	.363	.135	0	.441	.529	-0.62
	-43.5	-1.68E-12	.295	6.124	8.627	.999	.9969	181.	8.3E-9	2.01E5	.343	.139	0	0.030	.940	-1.11
CORE	-50.1	-1.61E-11	.296	6.806	8.776	0.999	.9971	172.	8.6E-7	4.07E5	.322	.158	0	0	.970	-1.79
	-61.7	-1.31E-10	.296	7.452	8.917	1.000	.9974	156.	8.5E-5	9.17E5	.312	.141	0	0	.894	-2.44
C Shell	-65.7	-2.18E-10	.296	7.613	8.942	1.000	.9988	74.	2.5E-4	1.19E6	.313	.069	0	0	.407	-2.60
	-73.8	-5.07E-10	.296	7.883	8.953	1.000	0.9998	9.	1.2E-3	2.07E6	.318	.011	0	0	.035	-2.87
	-83.0	-1.11E-9	.297	8.136	8.955	1.000	1.0000	3.	4.6E-3	3.73E6	.325	.004	0	0	0.005	-3.12
r_{m-i}	-96.1	-2.71E-8	0.297	8.424	8.956	1.000	1.0000	0.	1.9E-2	7.49E6	0.336	0.000	0	0	0	-3.41

TABLE 2

INTERNAL STRUCTURE OF A STAR WITH $M_t = 12.0\ M_\odot$, $M_{tc} = 1.0\ M_\odot$, $R_c = 9.98$ km, $X_{ph} = 0.70$, $Y_{ph} = 0.27$, $C_{ph} = 0.0$

(Note: $r_K = 10.00$ km, $M_{tK} = 1.000\ M_\odot$, $r_{m-i} = 9.92$ km; for details of notation see §I.e.)

Region	$r-r_K$ (m)	$M_{tr}-M_{tK}$ ($M_\odot$)	$\frac{2GM_{tr}}{c^2 r}$	log ρ (g/cm^3)	log T ($^\circ$K)	β_g	τ	L_r ($L_\odot$)	$L^{ov}-\mathcal{R}^2 L_r^{ov}$ ($L_\odot$)	L_r^{crit} ($L_\odot$)	∇_{ad}	∇_{rad}	∇	log v_t (cm/sec)	log v_s (cm/sec)	log v_{in} (cm/sec)
PHOTOSPHERE	7.50E11	10.90	4.69E-8	-8.397	3.462		0.667				0.118	0.148	0.148	2.69	5.66	
	7.43E11	10.80	4.69E-8	-8.191	3.598		3.92				.387	1.01	1.01	3.66	5.81	
	7.38E11	10.68	4.68E-8	-8.330	3.916		1590.				.104	76.5	0.836	5.45	5.90	
	6.71E11	9.44	4.60E-8	-8.127	4.200						.232	470.	.629	5.53	6.21	
	4.03E11	3.58	3.36E-8	-7.709	4.671						.254	23.9	.352	5.55	6.49	
STATIC ENVELOPE	3.28E10	5.45E-3	9.06E-8	-7.194	5.148						.263	2.55	.352	6.09	6.85	
	2.15E9	5.06E-6	1.37E-6	-6.699	5.617						.250	0.594	.265	6.64	7.38	
	1.35E8	6.84E-9	2.19E-5	-5.999	6.092						.250	.501	.252	7.19	7.95	
							$\frac{}{1-\mathcal{R}^2 L_r/L}$									
r_{o-m}	1.53E7	6.90E-11	1.93E-4	-5.243	6.504	9.21E-3	0	73547.	<< E-20	38301.	.250	.484	.251	7.57	8.40	2.79
	1.48E6	2.33E-12	1.98E-3	-3.996	7.040	4.04E-3	0	73691.	6.1E-21	39000.	.250	.474	.250	7.82	8.84	3.57
	4.04E5	9.70E-13	7.12E-3	-2.963	7.417	3.23E-3	0	74086.	9.1E-19	40411.	.250	.459	.250	7.85	9.08	3.65
	1.45E5	6.22E-13	0.0191	-1.958	7.762	3.01E-3	-0.001	75003.	2.0E-16	43448.	.250	.431	.250	7.78	9.26	3.50
INFLOWING ENVELOPE	5.64E4	4.32E-13	.0445	-0.969	8.095	2.95E-3	-0.001	77003.	4.8E-14	50043.	.250	.382	.250	7.67	9.43	3.25
	2.42E4	3.01E-13	.0864	-0.119	8.379	2.93E-3	-0.001	80545.	5.8E-12	61612.	.250	.324	.250	7.53	9.57	2.99
	1.03E4	1.93E-13	.146	+0.596	8.617	2.93E-3	0	86042.	4.0E-10	79400.	.250	.270	.250	7.28	9.68	2.74
H Shell begins	4.45E3	1.12E-13	.204	1.097	8.784	3.96E-3	+0.024	90228.	6.4E-7	59575.	.249	.366	.249	7.42	9.76	2.55
	2.51E3	7.29E-14	.236	1.324	8.858	8.84E-3	.100	86617.	1.5E-5	23150.	.247	0.857	.247	7.48	9.78	2.46
	883.	2.97E-14	.271	1.559	8.932	0.0217	.401	60407.	2.0E-4	9740.	.243	1.396	.243	7.40	9.81	2.36
	126.	4.61E-15	.292	1.688	8.972	.0334	.831	17518.	6.7E-4	6719.	.241	0.612	.241	7.16	9.82	2.30
	14.4	5.34E-16	.295	1.708	8.9782	.0356	.931	7222.	8.0E-4	6377.	.240	.288	.240	6.85	9.82	2.29
	5.56	2.07E-16	.295	1.710	8.9787	.0357	.939	6347.	8.1E-4	6351.	.240	.259	0.240	6.71	9.82	2.29
													X	Y	C	
KNEE	0	0	.295	1.711	8.9790	.0359	.945	5788.	8.2E-4	6336.	.240	.240	0.700	0.270	0	2.28
	-0.57	-2.54E-17	.295	1.905	8.9791	.0360	.964	3705.	8.2E-4	9817.	.240	.114	0.367	0.603	0	2.09
H Shell ends	-1.13	-7.36E-17	.295	2.302	8.9791	.0365	.986	1485.	8.2E-4	24194.	.240	.0267	0.021	0.949	0	1.69
	-3.82	-1.06E-15	.296	3.045	8.9791	.0491	.9971	301.	8.3E-4	1.16E5	.241	.0029	0	0.970	0	0.95
He Shell	-8.59	-1.07E-14	.296	3.819	8.9792	.159	.9992	85.9	8.3E-4	2.19E5	.247	.0005	0	0.949	0.021	0.18
	-12.5	-4.62E-14	.296	4.453	8.9792	.411	.9996	42.5	8.4E-4	2.28E5	.253	.0002	0	0.480	0.490	-0.46
HALO	-17.6	-3.70E-13	.296	5.385	8.9793	.843	.9998	22.1	8.5E-4	2.29E5	.283	.0002	0	0.022	0.948	-1.39
	-19.7	-8.66E-13	.296	5.732	8.9794	.926	.9998	20.1	8.5E-4	2.30E5	.299	.0004	0	0.006	0.959	-1.73
C Shell	-22.1	-2.08E-12	.296	6.068	8.9796	.968	.9998	18.4	8.6E-4	2.36E5	.309	.0007	0	0.002	0.940	-2.07
	-27.8	-1.15E-11	.296	6.667	8.9804	.994	.9999	9.5	8.8E-4	2.83E5	.310	.0015	0	0	0.491	-2.67
	-36.2	-6.33E-11	.296	7.220	8.9812	0.999	1.0000	1.2	9.7E-4	5.01E5	.306	.0007	0	0	0.032	-3.22
CORE	-49.7	-3.60E-10	0.297	7.776	8.9816	1.000	1.0000	0.1	1.9E-3	1.44E6	0.312	0.0003	0	0	0	-3.78

TABLE 3*

MODELS WITH M_{tc} = 1 $M_\odot$, R_c = 10.00 km, X_{ph} = 0.70, Y_{ph} = 0.27, C_{ph} = 0.0

Type Model*	M_t ($M_\odot$)	L ($L_\odot$)	T_{ph} (°K)	R_{ph} ($R_\odot$)	log T_{o-m} (°K)	$\dot{M}$ (10^{-8} $M_\odot$/yr)	L_{nuc}/L	r_K (km)	log ρ_K (g/cm^3)	log T_K (°K)	r_H-r_K (m)	log ρ_H (g/cm^3)	log T_H (°K)	$r_{He}-r_K$ (m)	log ρ_{He} (g/cm^3)	log T_{He} (°K)	r_C-r_K (m)	log ρ_C (g/cm^3)	Envelope Stable?*
G,R,α = 1	2.0	38220	2621	917	5.923	1.575	0.030	10.039	-1.871	8.098	-37	4.12	8.369	-41	5.61	8.529	-66	7.62	NO
G,R,α = 1	3.0	38430	2549	984	5.977	1.584	0.030	10.045	-1.817	8.111	-36	4.12	8.369	-40	5.61	8.530	-65	7.62	NO
G,R,α = 1	5.0	41740	2649	961	6.190	1.720	0.030	10.047	-1.267	8.249	-37	4.05	8.386	-41	5.60	8.537	-65	7.59	YES
G,R,α = 1	8.0	55680	2776	1016	6.374	2.286	0.030	10.024	-0.004	8.561	-47	3.35	8.569	-53	5.41	8.610	-75	7.46	YES
G,R,α = 1	9.0	60380	2809	1034	6.406	2.477	0.030	10.028	0.309	8.639	-58	3.10	8.643	-65	5.29	8.663	-87	7.41	YES
	MASS GAP																		
S,R,α = 1	11.5	71360	2882	1070	6.498	0.167	0.945	10.000	1.706	8.978	711	1.58	8.940	-12	4.44	8.978	-28	6.67	YES
S,R,α = 1	12.0	73530	2894	1077	6.504	0.165	0.947	10.000	1.711	8.979	725	1.59	8.940	-12	4.44	8.979	-28	6.66	YES
S,R,α = 1	16.0	90490	2978	1130	6.539	0.156	0.959	10.000	1.743	8.987	712	1.62	8.949	-12	4.42	8.987	-27	6.57	YES
S,R,α = 1	20.0	105600	3047	1168	6.563	0.150	0.966	10.000	1.766	8.992	731	1.64	8.953	-12	4.41	8.992	-26	6.51	YES
S,R,α = 1	25.0	123260	3114	1209	6.585	0.144	0.972	10.000	1.789	8.998	718	1.66	8.960	-11	4.40	8.998	-25	6.45	YES
G,N,α = 1	5.0	41770	2649	961	6.179	1.852	0.038	10.040	-2.071	8.026	-32	4.07	8.369	-38.	5.60	8.532	-72	7.59	YES
G,R,α = 0.5	5.0	38180	2209	1324	6.029	1.573	0.030	10.068	-1.693	8.145	-62	4.11	8.370	-66.	5.63	8.526	-93	7.69	YES
R,α = 1.5	5.0	IN MASS GAP; NO MODEL EXISTS																	

*In the first column, G means giant, S means supergiant, R means relativistic model, N means Newtonian mode, and α is the ratio of mixing length to pressure scale height. In the last column "ENVELOPE STABLE?" means "Is the static envelope stable against small, adiabatic, radial perturbations?" For other details of notation see §I.e.

TABLE 4*

EVOLUTIONARY SEQUENCE FOR A STAR OF M_t = 5 $M_\odot$, X_{ph} = 0.70, Y_{ph} = 0.27, C_{ph} = 0.0

M_{tc} ($M_\odot$)	R_c (km)	L ($L_\odot$)	T_{ph} (°K)	R_{ph} ($R_\odot$)	log T_{o-m} (°K)	$\dot{M}$ (10^{-8} $M_\odot$/yr)	L_{nuc}/L	r_K (km)	log ρ_K (g/cm^3)	log T_K (°K)	r_H-r_K (m)	log ρ_H (g/cm^3)	log T_H (°K)	$r_{He}-r_K$ (m)	log ρ_{He} (g/cm^3)	log T_{He} (°K)	r_C-r_K (m)	log ρ_C (g/cm^3)	Envelope Stable?*
0.4	12.172	24590	2734	696	6.569	3.028	0.100	12.398	0.421	8.524	-181	3.07	8.54	-209	5.16	8.62	-273	6.94	YES
0.8	11.255	36210	2659	889	6.298	2.121	0.045	11.323	-0.975	8.275	-57	3.87	8.40	-64	5.48	8.55	-98	7.36	YES
1.0	11.075	41730	2649	961	6.193	1.913	0.034	11.124	-1.329	8.219	-41	4.01	8.38	-46	5.56	8.54	-75	7.52	YES
1.4	10.680	54400	2654	1091	5.999	1.673	0.021	10.710	-1.505	8.229	-26	4.16	8.37	-29	5.68	8.52	-50	7.82	YES
1.6	10.250	61860	2670	1149	5.956	1.561	0.016	10.277	-1.329	8.300	-24	4.16	8.38	-26	5.73	8.52	-43	7.92	YES
1.625	9.299	62810	2672	1156	5.950	1.388	0.013	9.336	-1.153	8.364	-35	4.10	8.41	-37	5.75	8.53	-49	7.93	YES

*See footnote to Table 3.

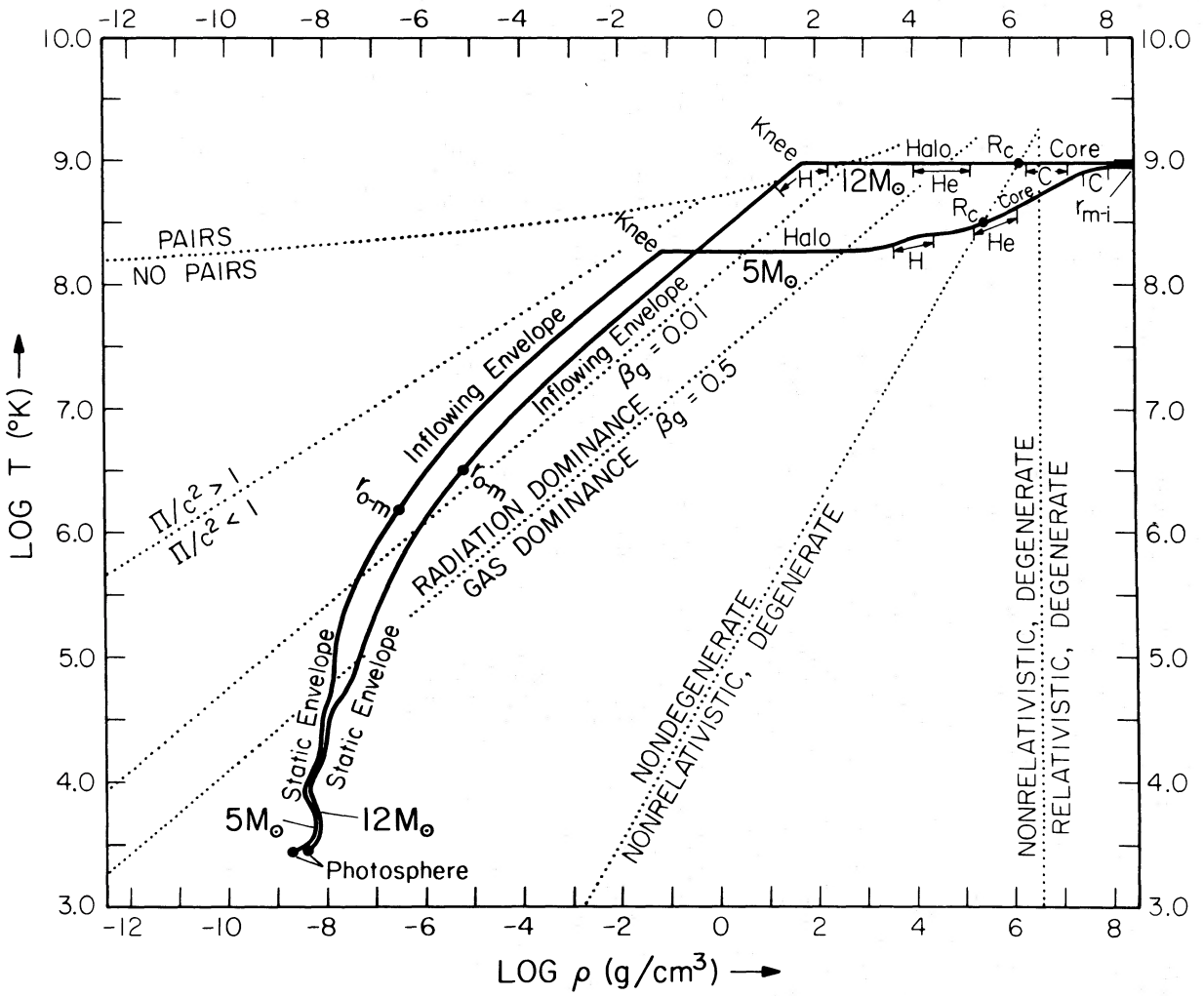

FIG. 2.—The internal distributions of density and temperature for a giant model with total mass $M_t = 5\ M_\odot$, and a supergiant with $M_t = 12\ M_\odot$. Both models have envelope abundances (≡photospheric abundances) $X_{ph} = 0.70$, $Y_{ph} = 0.27$, $C_{ph} = 0$, and core mass and radius $M_{tc} = 1\ M_\odot$, $R_c = 10$ km. Further details of the internal structures of these stars are given in Tables 1 and 2. The solid curves are the runs of density and temperature in the two models. Along these curves are marked several regions of the model which were described qualitatively in Fig. 1 (photosphere, static envelope, junction point r_{o-m} between outer and middle regions, inflowing envelope, knee, halo, junction point R_c between halo and core, core, and junction point r_{m-i} between middle and inner regions. Also shown along each curve are the locations of the hydrogen-, helium-, and carbon-burning shells.

The dotted lines are several regions of interest in the density-temperature plane: Above the "PAIRS—NO PAIRS" line the density of electron-positron pairs exceeds that of ionization electrons; below, ionization electrons dominate. [This curve is given analytically by $y = 0.354$ where y is defined by eq. (A.8) of the Appendix.] The "RADIATION DOMINANCE–GAS DOMINANCE" line is the line where $\beta_g \equiv$ (gas pressure)/(radiation pressure plus gas pressure) is 0.5. For further details on notation see § Ie.

Consider the forces which act on the plasma (gas) in the nondegenerate region $r > R_c$. The pull of gravity is counteracted by the plasma's own pressure-buoyancy force and by the force of outflowing radiation:

$$\begin{pmatrix}\text{gravitational force}\\ \text{per unit volume}\end{pmatrix} \equiv -\frac{GM_r\rho}{r^2}\mathcal{G}\mathcal{H}_g\mathcal{V} = \frac{1}{\mathcal{V}}\frac{dP_g}{dr} - \frac{\kappa\rho L_r^{\rm rad}}{4\pi r^2 c}\,. \tag{4.1}$$

Here $\mathcal{H}_g$ is the relativistic enthalpy correction factor for the gas only,

$$\mathcal{H}_g \equiv 1 + (\Pi_g - B + P_g/\rho)/c^2 \tag{4.2}$$

(cf. eq. [T, 6e]); $L_r^{\rm rad}$ is the locally measured luminosity carried by diffusing radiation

$$L_r^{\rm rad} \equiv L_r - 4\pi r^2 F_{\rm conv}\,; \tag{4.3}$$

and all other quantities have been defined earlier (cf. § I*e*). This force-balance equation can be derived either from first principles, or from the relativistic equations of stellar structure (2.20a, h, i), (2.28), (4.2), (4.3), (T, 6d, e), (T, 8a, b), (T, 9a), and (T, 10a). By analogy with Newtonian theory, it is convenient to rearrange the force-balance equation (4.1) as follows:

$$\frac{1}{\mathscr{V}}\frac{dP_g}{dr} = -\frac{GM_r\rho}{r^2}\mathscr{G}\mathscr{H}_g\mathscr{V}\left(1 - \frac{L_r^{\rm rad}}{L_r^{\rm crit}}\right), \tag{4.4a}$$

where

$$L_r^{\rm crit} \equiv 4\pi GcM_r\kappa^{-1}\mathscr{G}\mathscr{H}_g\mathscr{V} \tag{4.4b}$$

is the "critical luminosity" above which the force of outflowing radiation on the plasma exceeds the force of gravity. Equation (4.4a) shows that the scale height for the gas pressure is

$$\begin{aligned} H_{P_g} &= \frac{-\mathscr{V}\,dr}{d\ln P_g} = r\left(\frac{P_g}{\rho c^2}\right)\left(\frac{GM_r}{c^2 r}\right)^{-1}\mathscr{G}^{-1}\mathscr{H}_g^{-1}\mathscr{V}^{-1}\left(1 - \frac{L_r^{\rm rad}}{L_r^{\rm crit}}\right)^{-1} \\ &= (6\times 10^{-4}r)\left(\frac{T}{10^9\ {\rm K}}\right)\left(\frac{1}{\mu}\right)\left(\frac{r}{10\ {\rm km}}\right)\left(\frac{M_r}{M_\odot}\right)^{-1}\mathscr{G}^{-1}\mathscr{H}_g^{-1}\mathscr{V}^{-1}\left(1 - \frac{L_r^{\rm rad}}{L_r^{\rm crit}}\right)^{-1}. \end{aligned} \tag{4.5}$$

[Here use is made of the plasma equation of state $P_g = (\rho/\mu m_{\rm H})kT$.]

As one moves outward through the star, this equation for H_{P_g} first becomes valid where electron degeneracy turns off (at $\rho \sim 10^6$ g cm^{-3}, $r = R_c$). At that point all quantities on the right-hand side of the equation are of order unity, so $H_{P_g}/r \sim 6\times 10^{-4}$. Thus, the plasma just above the core's edge has the extremely small scale height of a hot ($T = 10^9$ K) neutron-star atmosphere: $H_{P_g} \sim 1$ meter. Physically this scale height is governed by the inability of the mean particle kinetic energies, $kT \sim 10^{-4}m_{\rm H}c^2$, to compete with the extremely strong pull of gravity, $GM_c/c^2r \sim 0.1$.

The "halo" of our models is the region just above the core where $H_{P_g} \sim 1$ meter. As one moves outward through the halo a distance $\sim$15 meters, the density drops to $\sim 10^6 \times e^{-15} \sim 1$ g cm^{-3}. This rapid density drop cannot continue for many more meters if the star is to support a massive envelope around itself. Something must happen soon to increase H_{P_g}/r from $\sim 6\times 10^{-4}$ to ~ 1. Equation (4.5) shows two ways to increase H_{P_g}/r: (i) by a decrease of the mean molecular weight to $\sim 10^{-3}$ due to a profuse turn-on of electron-positron pairs; (ii) by an increase of $L_r^{\rm rad}/L_r^{\rm crit}$ to near unity so that the force of outflowing radiation on the plasma strongly counteracts the inward force of gravity. In all of our models the radiation force (case ii) is responsible for the increase in H_{P_g}/r. It is conceivable—but seems unlikely to us—that one could build models of type (i), where H_{P_g}/r increases due to profuse pairs.

In our giant models, as one moves outward through the halo (where energy transport is all radiative), gravitational energy release drives $L_r \equiv L_r^{\rm rad}$ up higher and higher. Ultimately, at $\rho \sim 1$ g cm^{-3}, the luminosity L_r goes supercritical and H_{P_g}/r becomes ~ 1. Very shortly before this point the force of outflowing radiation on the plasma becomes so great that it begins to drive convection.[1] The onset of convection marks the end of the halo and the beginning of the convective envelope.

Throughout the strong-gravity region of the convective envelope, the plasma is protected against the pull of gravity by the force of outflowing radiation ($1 - L_r^{\rm rad}/L_r^{\rm crit} \sim 10^{-3}$). Because the radiative luminosity is so extremely close to critical, the star is forced to remain convective throughout this region. Ultimately, with increasing radius, gravity weakens enough that there might be some hope of the plasma supporting itself without the help of radiation forces. However, the outflowing luminosity cannot now be shut off. It is pouring outward with a rate L_r designed to counterbalance gravity at small radii, $L_r \approx L_r^{\rm crit}$(strong-gravity region); and with ever-increasing r and ever-decreasing T the opacity is rising higher and higher, driving $L_r^{\rm crit}$ lower and lower. Thus, the star remains supercritical (and therefore convective) all the way from its knee out to the photosphere.

One knows from the theory of stellar envelopes that because our stars have very deep convection they must be near the Hayashi track of the H-R diagram where photospheric temperatures are low:

$$T_{\rm ph} \lesssim 3000\ {\rm K}. \tag{4.6a}$$

The above argument shows, moreover, that the luminosities of our stars must be

$$L \sim L_r^{\rm crit}(\text{strong-gravity region}) \sim 4\pi GcM_\odot/\kappa_{\rm es} \sim 4\times 10^4\, L_\odot. \tag{4.6b}$$

These numbers agree with the detailed models of Tables 1–4.

We suspect, but are not certain, that it is impossible to construct equilibrium models of stars with neutron cores and massive envelopes that lie elsewhere in the H-R diagram. The extreme force of gravity near the core probably always enforces deep convection and very high L—and thereby red-supergiant surface features.

[1] The Newtonian proof (Joss, Salpeter, and Ostriker 1973), that convection sets in before L_r becomes supercritical, is easily generalized to relativity theory.

Using the above information about the stellar structure, we can understand semiquantitatively the flow of energy inside the star: Mass flows from the static envelope, through the inflowing envelope, into the halo, and thence into the core. In the inflowing envelope, because of inefficiency of convection, the temperature gradient is slightly superadiabatic, so the inflowing matter gets heated not only by adiabatic compression due to gravity, but also by the absorption of some of the upflowing luminosity L_r. Mathematically, in the equation of energy generation (2.20d) $d\Pi/dM_r - (P/\rho^2)(d\rho/dM_r)$ is negative due to superadiabaticity, so $L_r\mathscr{R}^2$ (the redshifted luminosity) increases inward. Equivalently, in the equation of energy conservation (2.43) superadiabaticity means that $\mathscr{H}\mathscr{R}$ increases inward, so $L_r\mathscr{R}^2$ also increases inward.

By the time it reaches the knee, the inflowing matter contains an enormous amount of internal energy, almost all of it tied up in radiation:

$$(\mathscr{H}\mathscr{R})_K > (\mathscr{H}\mathscr{R})_{\rm ph} \Rightarrow \frac{4}{3}\frac{\Pi_{\rm rad}}{c^2} \approx \frac{\Pi + P/\rho}{c^2} > (1 - B_{\rm ph}/c^2)[(1 - 2GM_{tc}/c^2R_c)^{-1/2} - 1] \sim 0.2. \tag{4.7}$$

[Here we have used expressions (T, 6e) and (2.36) for $\mathscr{H}$ and $\mathscr{R}$, together with the fact that because the knee is so close to the core boundary, the redshift factor $\mathscr{R}$ is very nearly the same at the knee as at the core boundary.] At the knee the temperature gradient goes very subadiabatic (in fact, nearly isothermal), so the contracting matter begins to release its huge store of thermal energy, converting it into outflowing radiation. Because its temperature is now remaining constant, its specific internal energy $\Pi \approx aT^4/\rho$ falls off as $1/\rho$. After the density has increased by only a factor 10 above $\rho_{\rm knee}$, 90% of the stored energy has been converted into luminosity L_r. After several more decades of density increase, nuclear burning begins to occur, producing further luminosity (but much less than was produced by gravity and released just below the knee). By the time the flowing matter gets inside the core, essentially all the star's luminosity has been accounted for; L_r has dropped nearly to zero. Overall, the contribution of gravitational contraction to the total luminosity of the star is

$$L_{\rm grav} = \dot{M}c^2(1 - B_{\rm ph}/c^2)[1 - (1 - 2GM_{tc}/R_cc^2)^{1/2}] \tag{4.8a}$$

(cf. eq. [2.43] and associated discussion); and the contribution of nuclear burning is

$$L_{\rm nuc} = \dot{M}c^2(1 - 2GM_{tc}/R_cc^2)^{1/2}0.007118[0.936\,X_{\rm ph} + (X_{\rm ph} + Y_{\rm ph})/11.0 + (X_{\rm ph} + Y_{\rm ph} + C_{\rm ph})/13]. \tag{4.8b}$$

The ratio $L_{\rm nuc}/L \equiv L_{\rm nuc}/(L_{\rm nuc} + L_{\rm grav})$ is shown for various models in Tables 3 and 4.

For a detailed example of these features of energy flow, see the columns labeled $r - r_K$, ρ, and $1 - \mathscr{R}^2L_r/L$ in Table 1.

Non–nuclear-burning neutrino losses are totally negligible ($\ll 1\,L_\odot$) in the outer and middle regions ($\rho < 3 \times 10^8$ g cm^{-3}) of all our models; cf. Tables 1 and 2. We have not made a thorough search for models with high neutrino losses; but we suspect that high losses are incompatible with stellar equilibrium as well as stability.

b) Structure of the Halo and Sharpness of the Knee

The halos of our giant models are remarkably isothermal, and the transition through the knee into a superadiabatic temperature gradient is remarkably sharp (see Fig. 2). These features can be understood as follows:

To avoid issues of radially changing chemical composition, consider that region of the halo which lies outside the hydrogen-burning shell ($\rho < 3 \times 10^3$ g cm^{-3} for the 5 $M_\odot$ model of Fig. 2). Here the pressure and internal energy due to gas and radiation are

$$P_g = \frac{\rho kT}{\mu m_{\rm H}}\,; \quad \Pi_g = \frac{3}{2}\frac{P_g}{\rho}\,; \quad P_{\rm rad} = \frac{1}{3}aT^4; \quad \Pi_{\rm rad} = \frac{3P_{\rm rad}}{\rho}\,;$$

$$\mu = \left(\frac{1}{\mu_e} + \frac{1}{\mu_{\rm ion}}\right)^{-1} = \left(\frac{1}{2} + \frac{3X_{\rm ph}}{2} + \frac{Y_{\rm ph}}{4} + \frac{Z_{\rm ph}}{16}\right)^{-1} = \text{const.} \tag{4.9a}$$

Because the halo is so thin in radius and contains so little mass, throughout it we can set $r = R_c$, $M_{tr} = M_{tc}$; and thence

$$\mathscr{V}^{-1} = \mathscr{R} = \mathscr{R}_c = (1 - 2GM_{tc}/c^2R_c)^{1/2} \tag{4.9b}$$

(cf. eq. [2.36]). Also, because $P/c^2 \lesssim \rho \ll M_{tc}/4\pi R_c^3$ throughout the halo, and because nuclear binding energies and particle kinetic energies are small compared to $m_{\rm H}c^2$, we can approximate

$$\mathscr{G} = M_{tc}/M_r, \quad \mathscr{H}_g = 1 \tag{4.9c}$$

(cf. eqs. [T, 6c] and [4.2]). Finally, because all luminosity is carried radiatively in the halo, we can set $L_r^{\rm rad} = L_r$.

By using the above relations we can rewrite the force-balance equation (4.4a) for the plasma in the halo as

$$\frac{dP_g}{dr} = -\frac{g_c}{\mathscr{R}_c}\rho\left(1 - \frac{L_r}{L_r^{\rm crit}}\right), \tag{4.10a}$$

where g_c is the acceleration of gravity at the edge of the core,

$$g_c \equiv (GM_{tc}/R_c^2)\mathscr{R}_c^{-1} . \tag{4.10b}$$

The analogous equation of force balance for the radiation is obtained by setting $P_{\rm rad} = P - P_g$, by taking the difference of equations (2.20i, a) and (4.10a), and by invoking the relations (4.9b, c), (4.10b), and $\mathscr{H} - 1 \approx 4P_{\rm rad}/\rho c^2$ [cf. eqs. (T, 6e) and (4.9a, c)]:

$$\frac{dP_{\rm rad}}{dr} = -\frac{4g_c}{\mathscr{R}_c}\frac{P_{\rm rad}}{c^2} - \frac{g_c}{\mathscr{R}_c}\rho\frac{L_r}{L_r^{\rm crit}} . \tag{4.11}$$

The first term on the right-hand side is a gravitational redshift term; it can be neglected because of the thinness of the halo ($r_K - R_c \ll R_c$):

$$dP_{\rm rad}/dr = -(g_c/\mathscr{R}_c)\rho(L_r/L_r^{\rm crit}) . \tag{4.11'}$$

By taking the ratio of the force-balance equations (4.10a) and (4.11') and combining with the equation of state (4.9a), we obtain

$$d\ln T/d\ln\rho = (4\gamma_L/\gamma_g - 1)^{-1} , \tag{4.12a}$$

where

$$\gamma_L \equiv L_r^{\rm crit}/L_r - 1 = \beta_L/(1-\beta_L) , \qquad \gamma_g \equiv P_g/P_{\rm rad} = \beta_g/(1-\beta_g) . \tag{4.12b}$$

We shall see below that $\gamma_L \gg \gamma_g$ throughout the halo, except very near the knee and near the nuclear-burning shells; thus, the halo must be nearly isothermal ($d\ln T/d\ln\rho \ll 1$).

The opacity in the halo is due, almost entirely, to electron scattering and thus depends on temperature but not density (eq. [2.32])—and is essentially constant throughout the halo. Thus, $L_r^{\rm crit}$ (eq. [4.4b]) is also essentially constant, with value

$$L_r^{\rm crit} = \frac{4\pi GcM_{tc}}{\mathscr{R}_c\kappa_{\rm es}} = \frac{3.2\times10^4\,L_\odot}{\mathscr{R}_c G(T_K)}\frac{M_{tc}}{M_\odot}\frac{2}{1+X_{\rm ph}} , \tag{4.13}$$

where $G(T_K)$ is the Klein-Nishina correction function for the electron scattering opacity, evaluated at the temperature of the knee T_K. The knee occurs where the temperature gradient becomes adiabatic; thus

$$d\ln T/d\ln\rho = (\partial\ln T/\partial\ln\rho)_S = \tfrac{1}{3} \text{ at knee} . \tag{4.14a}$$

(Here we have used the fact that $P_{\rm rad} \gg P_g$ near the knee, so that the adiabats are $T^3/\rho = $ const.) Equations (4.14a) and (4.12a) show that

$$\gamma_L = \gamma_g \text{ at knee} ; \qquad \gamma_L > \gamma_g \text{ in halo} . \tag{4.14b}$$

The value of γ_L in the halo is governed by L_r, which is determined by the equation of energy conservation:

$$L_r = L_r^{\rm nuc} + \mathscr{R}_c^{-1}\dot{M}(\Pi_{\rm rad} + P_{\rm rad}/\rho) = L_r^{\rm nuc} + \text{const.}/\rho . \tag{4.15}$$

[See eqs. (2.43), (4.8b), and (T, 6e) specialized to the case $r - R_c \ll R_c$; $B = B_{\rm ph}$, $X = X_{\rm ph}$, and $\Pi_{\rm gas} + P_{\rm gas}/\rho$ radially constant because of isothermality. Here $L_r^{\rm nuc}$ is the total contribution of nuclear burning to L_r in the halo:

$$L_r^{\rm nuc} = \mathscr{R}_c^{-2}L_{\rm nuc} = \mathscr{R}_c^{-1}\dot{M}c^2\cdot0.007188[0.936\,X_{\rm ph} + (X_{\rm ph}+Y_{\rm ph})/11.0 + (X_{\rm ph}+Y_{\rm ph}+C_{\rm ph})/13]; \tag{4.16}$$

cf. eq. (4.8b).] By combining equations (4.15) and (4.12b), using (4.14b) to evaluate the constant in (4.15), using the constancy of $L_r^{\rm crit}$, and ignoring a factor γ_{gK} where it is unimportant, we obtain

$$\gamma_L = \frac{(\rho/\rho_K)(\gamma_{gK}+1)}{1+\beta_{\rm nuc}(\rho/\rho_K - 1)} - 1 , \qquad \beta_{\rm nuc} \equiv \frac{L_r^{\rm nuc}}{L_r^{\rm crit}} \sim 0.03 . \tag{4.17}$$

Here ρ_K and γ_{gK} are the values of ρ and γ_g at the knee, and $\beta_{\rm nuc} \sim 0.03$ because

$$L_r^{\rm nuc} = \mathscr{R}_c^{-2}L_{\rm nuc} \sim 0.030\,\mathscr{R}_c^{-2}L \sim 0.030\,L_r(\text{knee}) \approx 0.030\,L_r^{\rm crit} .$$

Because $\gamma_g = \gamma_{gK}(\rho/\rho_K)$ in the isothermal region, we have

$$\frac{\gamma_L}{\gamma_g} = 1 + \frac{(\rho/\rho_K - 1)(1 - \beta_{\rm nuc} - \beta_{\rm nuc}\gamma_{gK}\rho/\rho_K)}{[1+\beta_{\rm nuc}(\rho/\rho_K - 1)](\gamma_{gK}\rho/\rho_K)} . \tag{4.18}$$

The isothermal region is that region in which $\gamma_L/\gamma_g \gg 1$ (cf. eq. [4.12a]). Equation (4.18) shows that it extends over the range

$$5 \times 10^{-4} \sim \gamma_{gK} \ll (\rho/\rho_K - 1) \ll 1/(\beta_{\rm nuc}\gamma_{gK}) \sim 7 \times 10^{+4} . \tag{4.19}$$

The ρ-T curve for the 5 $M_\odot$ star in Figure 2 demonstrates this: At the left end of the halo the termination of isothermality is so sharp ($\Delta\rho/\rho \sim \gamma_{gK} \sim 5 \times 10^{-4}$) that the slope of the ρ-T curve looks discontinuous. Toward the right isothermality ends at $\rho \sim 2 \times 10^4 \rho_K \sim 10^3$ g cm^{-3}. The above analysis diagnoses correctly small departures from isothermality; but as the departures become significant ($d \ln T/d \ln \rho \sim 0.1$), the analysis produces serious errors.

The density-radius relation in the isothermal region can be derived by combining the plasma equation of state (4.9a) and expressions (4.12b), (4.17) for $L_r/L_r^{\rm crit}$ with the plasma force-balance equation (4.10a), and then integrating. The result is

$$\rho - \rho_K = \text{constant} \times \exp\left(\frac{r_K - r}{\mathscr{R}_c H_h}\right) , \tag{4.20a}$$

where H_h is the value of the gas-pressure scale height (4.5) a few meters below the knee where $L_r = L_r^{\rm nuc}$:

$$H_h = R_c\left(\frac{kT_K}{\mu m_{\rm H} c^2}\right)\left(\frac{GM_{tc}}{c^2 R_c}\right)^{-1}\frac{\mathscr{R}_c}{1-\beta_{\rm nuc}} = (6.22\text{ m})\left(\frac{T_K}{10^9\text{ K}}\right)\left(\frac{R_c}{10\text{ km}}\right)^2\left(\frac{M_{tc}}{M_\odot}\right)^{-1}\frac{\mathscr{R}_c}{\mu(1-\beta_{\rm nuc})} . \tag{4.20b}$$

For the 5 $M_\odot$ star of Table 1 and Figure 1 this formula gives $\mathscr{R}_c H_h = 1.30$ meters. The density profile (4.20a) agrees rather well with the numerical model of Table 1 inside its realm of validity (eq. [4.19]). For example, it describes within a few percent accuracy the increase in density scale height from $H_\rho = H_h = 1.55$ meters deep in the halo to $H_\rho = H_h(1 - \rho_K/\rho)^{-1} = 50$ meters at $1 - \rho_K/\rho = 3 \times 10^{-2}$. However, very near the knee (at $1 - \rho_K/\rho \sim \gamma_{gK} = 5 \times 10^{-4}$), it breaks down because of the breakdown in isothermality ($d \ln T/d \ln \rho$ no longer $\ll 1$).

Unfortunately, in the neighborhood of the knee there is a serious omission in the physics which we have put into our analysis: We have ignored the possibility of "convective overshoot" in which turbulent cells plow through the knee and into the upper layers of the halo before being stopped by pressure buoyancy forces.

We can estimate the effects of convective overshoot in our 5 $M_\odot$ model (Table 1) as follows: Just above the knee the mixing length (assumed equal to pressure scale height) is $l_t \approx R_c/4 = 2.5$ km (cf. eq. [4.26] below and recall that $P \propto T^4$). Table 1 shows that convective cells within this distance of the knee have typical velocities of $v_t \approx 10^{7.8}$ cm s^{-1}. Suppose that a small cell moving downward with this speed hits the knee, and that when it hits it has the same density and temperature, ρ_K and T_K, as its surroundings. Because the cell's velocity v_t is far less than its sound speed ($v_s \approx 10^{9.85}$ cm s^{-1}), it maintains pressure equilibrium with its surroundings as it penetrates the halo. Pressure equilibrium means temperature equilibrium since $P_{\rm rad} \gg P_{\rm gas}$, which means constancy of temperature since the halo is isothermal. Assuming negligible heat exchange between the cell and its surroundings (T^3/ρ constant in cell), we conclude that the cell maintains constant density, $\rho_{\rm cell} = \rho_K$, as it penetrates the halo. Consequently, its deceleration rate as it moves through the halo is given by

$$\rho_K \mathscr{R}_c^{-1} dv/dt = -g_c(\rho - \rho_K) ,$$

where g_c is the (constant) acceleration of gravity throughout the halo (eq. [4.10b].) Since $v = -\mathscr{R}_c^{-2} dr/dt$, and since the density profile has the form (4.20a), we can rewrite this deceleration equation in the form

$$dv^2/d(\rho - \rho_K) = -2g_c H_h/\rho_K . \tag{4.21}$$

Integrating this equation and imposing the boundary condition $v = v_t$ at $\rho = \rho_K$, we obtain for the density $\rho_{\rm overshoot}$ at which the cell halts its plunge and begins to rise:

$$\frac{\rho_{\rm overshoot}}{\rho_K} - 1 = \frac{v_t^2}{2g_c H_h} = \tfrac{1}{2}(1 - \beta_{\rm nuc})\frac{v_t^2}{c^2}\frac{\mu m_{\rm H} c^2}{kT_K} . \tag{4.22}$$

For our 5 $M_\odot$ model, with $\beta_{\rm nuc} = 0.028$, $v_t = 10^{7.8}$ cm s^{-1}, $\mu = 0.62$, and $T_K = 10^{8.25}$ K this gives $\rho_{\rm overshoot}/\rho_K \approx 1.08$. Cells moving 3 times as fast will penetrate 10 times farther, i.e., to $\rho_{\rm overshoot}/\rho_K \approx 2$.

The above estimates suggest that convective overshoot is of some, but not great, importance. However, the following factors make this conclusion somewhat uncertain: (i) We evaluated the convective overshoot assuming a small convective cell, but the size of a typical cell just above the knee is probably $\sim R_c/10 \sim 1$ km, which is far greater than the scale height (a few tens of meters) of the region into which the cell penetrates. (ii) The region of overshoot is the region of greatest gravitational energy release: the energy release between ρ_K and ρ is

$$\Delta L_r = (L_r^{\rm crit} - L_r^{\rm nuc})(1 - \rho_K/\rho) ; \tag{4.23}$$

cf. eq. (4.15). A serious modification of the temperature distribution in this region due to overshoot will seriously affect the details of gravitational energy release, and will thereby affect the average density profile and the pressure-buoyancy force on the convective cell, and might thus seriously affect our above estimates.

Obviously, a detailed study of overshoot is needed.

In this discussion of the halo, turn attention now to the nuclear-burning shells. Because of the extremely small scale height in the halo and in the outer layers of the core, the nuclear-burning shells are very thin: typically (physical thickness) $= \mathscr{R}_c^{-1}\Delta r \sim 2$ meters for the hydrogen shell, 4 meters for the helium shell, and 20 meters for the carbon shell (see Table 1). The time required for matter to contract through these shells is $\mathscr{R}_c^{-1}\Delta r/v_{\rm in} \sim 10$ s for the hydrogen shell, ~ 30 minutes for the helium shell, and ~ 10 days for the carbon shell. Note that the electrons are nondegenerate in the hydrogen shell, slightly degenerate in the helium shell, and fully degenerate in the carbon shell. However, these conclusions, particularly concerning the hydrogen shell, are somewhat uncertain because of inadequacy of our nuclear-burning rates (cf. § V). On the other hand, $L_{\rm nuc}/L \approx 0.030$ is so small that errors in our treatment of nuclear burning are probably unimportant for the overall structure of the star.

c) *Structure of the Inflowing Envelope*

In the inner regions of the inflowing envelopes of our giant stars (10^7 K $\lesssim T \lesssim T_K$) convection is fairly efficient, so the temperature gradient is not far from adiabatic; cf. Table 1, where adiabaticity would mean constancy of β_g, and Figure 2 where adiabaticity would mean a T-ρ curve parallel to the $\beta_g =$ constant lines. (One must not diagnose adiabaticity from $\nabla - \nabla_{\rm ad}$ in regions where $\beta_g \ll 1$.)

By approximating the temperature gradient as adiabatic, we can derive simple expressions for the structure of the inflowing envelope. Adiabaticity of the flow implies (by virtue of the relativistic Bernoulli equation, or by eq. [2.43] with $\mathscr{R}^2 L_r$ constant) that $\mathscr{H}\mathscr{R}$ is independent of radius. Because $\beta_g \ll 1$ and because nuclear binding energies can be ignored, equation (T, 6e) for $\mathscr{H}$ reduces to $1 + (4aT^4)/3\rho c^2$. By combining this expression for $\mathscr{H}$ with the relation

$$\beta_g = P_g/P_{\rm rad} = (3k/\mu m_{\rm H} a)(\rho/T^3)$$

and with expression (2.36) for $\mathscr{R}$, and by setting $\mathscr{H}\mathscr{R} = (\mathscr{H}\mathscr{R})_K$, we obtain

$$\frac{4}{\beta_g}\frac{kT}{\mu m_{\rm H} c^2} = \left(1 + \frac{4}{\beta_g}\frac{kT_K}{\mu m_{\rm H} c^2}\right)\left(\frac{1 - 2GM_{tc}/c^2R_c}{1 - 2GM_{tc}/c^2 r}\right)^{1/2} - 1 . \tag{4.24}$$

In order that the temperature T not go negative and not go isothermal at $r \gg r_K$, the knee temperature must satisfy

$$\frac{4}{\beta_{gK}}\frac{kT_K}{\mu m_{\rm H} c^2} = \frac{1}{(1 - 2GM_{tc}/c^2R_c)^{1/2}} - 1 . \tag{4.25}$$

Deviations from this relation are a measure of the deviation from adiabaticity. For the 5 $M_\odot$ model of Table 1 this relation predicts $\log T_K = 8.217$ compared to an actual value of $\log T_K = 8.249$. Using relation (4.25) we can rewrite equation (4.24) for the temperature profile as

$$\frac{4}{\beta_g}\frac{kT}{\mu m_{\rm H} c^2} = \frac{1}{(1 - 2GM_{tc}/c^2 r)^{1/2}} - 1 \approx \frac{GM_{tc}}{c^2 r} , \tag{4.26}$$

where "$\approx$" is the Newtonian limit.

Note that $T \propto 1/r$ implies $\rho \propto 1/r^3$, which means that M_r and M_{tr} increase only logarithmically with radius

$$M_{tr} - M_{tK} \approx 4\pi\rho_K R_c^3 \ln(r/r_K) . \tag{4.27}$$

This accounts for the very small amount of mass contained in the inflowing envelope (third column of Table 1).

d) *Structure of the Outer Region*

The outer regions of our models ($r > r_{o-m}$; static envelope, photosphere, atmosphere) are very similar to the outer regions of red supergiants with white-dwarf cores or nondegenerate cores. Therefore, we shall not comment on their detailed structures or on their sensitivity to the choice of mixing length (Table 3).

However, it is very important to notice that the luminosities and photospheric temperatures, L and $T_{\rm ph}$, are exceedingly insensitive to the details of the core, halo, and inflowing envelope. L and $T_{\rm ph}$ are fixed almost completely by the total mass M_t, the core mass M_{tc}, and the envelope composition $X_{\rm ph}$, $Y_{\rm ph}$, $C_{\rm ph}$. Compare, for example, the following three models with the same M_t, M_{tc}, $X_{\rm ph}$, $Y_{\rm ph}$, $C_{\rm ph}$, and ratio of mixing length to pressure scale height: the third model in Table 3 and the third model in Table 4 (relativistic models with different core radii), and the eleventh model in Table 3 (which is Newtonian). Despite the difference in their inflowing envelopes, halos, and cores, their luminosities and photospheric temperatures agree almost exactly.

Figure 3 explains this remarkable fact. Figure 3 is an H-R diagram for static stellar envelopes near the Hayashi track of a 5 $M_\odot$ star. All the curves in Figure 3 were constructed using Paczynski's computer program GOB for static stellar envelopes (§ II*c*), with no attempt to join the envelopes onto any kind of core. Notice the extremely narrow range of photospheric temperatures on the horizontal axis.

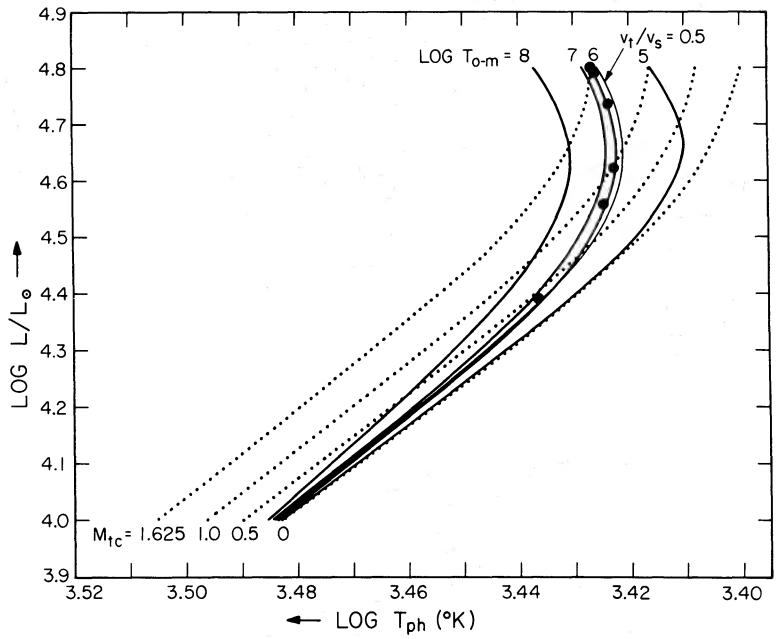

FIG. 3.—H-R diagram (luminosity versus photospheric temperature) for stars of total mass $M_t = 5\ M_\odot$, envelope abundances $X_{ph} = 0.70$, $Y_{ph} = 0.27$, and ratio of mixing length to pressure scale height $l_t/H_P = 1$. Each point in the L-T_{ph} diagram corresponds to a unique static envelope constructed by the prescription of § IIc. Each dotted curve is a region of constant core mass, $M_{tc} \equiv M_t - M_{env}$. The curve $M_{tc} = 0$ was calculated by extrapolation from $M_{tc} > 0$. Each thick solid curve is a region of constant temperature T_{o-m} at the base of the envelope (radius r_{o-m} defined by eq. [2.1]). To the left of the thin solid curve the turbulent velocity of convection is less than half the adiabatic sound velocity throughout the static envelope. To the right, $v_t > v_s/2$ near the base of the envelope—and therefore we are not justified in our use of subsonic mixing-length theory. The large dots are the surface properties of the six stellar models of Table 4.

The absolute temperatures and luminosities along the various curves are unreliable because of uncertainties in opacities and mixing length (which is here assumed equal to pressure scale height). However, the temperature and luminosity differences between various curves should be somewhat reliable.

The envelopes of Figure 3 can be joined onto a variety of types of cores. In the case of a white-dwarf core with hydrogen-burning shell source, the base of the static envelope, r_{o-m} of equation (2.1), is near or inside the shell source; thus $\log T_{o-m} \sim 7$ to 8 and stars with white-dwarf cores typically lie between the solid curves 8 and 7 of Figure 3.

In the case of a neutron core, the temperature falls off roughly as $1/r$ between r_K and $r_{o-m} \sim 10^3\ r_K$; and because $T_K < 10^9$ K, we must have $T_{o-m} \lesssim 10^6$ K. In fact, all of our detailed giant models (Tables 3 and 4) have $5.9 \lesssim \log T_{o-m} \lesssim 6.4$. In the envelope H-R diagram (Fig. 3) such models lie along an extremely narrow strip, $\Delta \log T_{ph} \approx 0.001$; and for given core mass M_{tc}, the luminosity within this strip varies by only $\Delta \log L \sim 0.02$. Thus, to within $\Delta \log T_{ph} \approx 0.001$ and $\Delta \log L \sim 0.02$, the envelope is oblivious of the details of the core and halo.

This behavior is due to the well-known fact that as one moves rightward in the H-R diagram, approaching the Hayashi forbidden region, the characteristics of the base of the envelope change extremely rapidly.

The above discussion shows that, for given L, the photospheric temperature is not even sensitive to the difference between a white-dwarf core and a neutron core. The star with a neutron core will be redder by only $\Delta \log T_{ph} \sim 0.01$.

V. DETAILS OF THE STELLAR STRUCTURE: SUPERGIANTS AND MASS GAP

Consider a sequence of models with fixed core properties (M_{tc}, R_c) and successively higher total mass M_t—e.g., the sequence in Table 3. The low-mass models have "giant" structures of the type discussed in § IV. The high-mass models have "supergiant" structures (convective envelope dips into hydrogen-burning shell, and most of the energy generation is by hydrogen burning rather than gravitational contraction). Between the giant and supergiant models there is a "mass gap" in which our computations have failed to produce any equilibrium configurations.

This peculiar situation can be understood as follows (see Fig. 4). The critical luminosity L_r^{crit} in the inflowing envelope has the form

$$\mathscr{R} L_r^{crit} = 4\pi G c M_{tc}/\kappa_{es} \tag{5.1}$$

(eqs. [4.4b], [4.9b, c]), where κ_{es} is the electron-scattering opacity

$$\kappa_{es} = (0.4\ \mathrm{cm^2/g})[(1 + X_{ph})/2](1 + 2n_+/n_e)G(T) \tag{5.2}$$

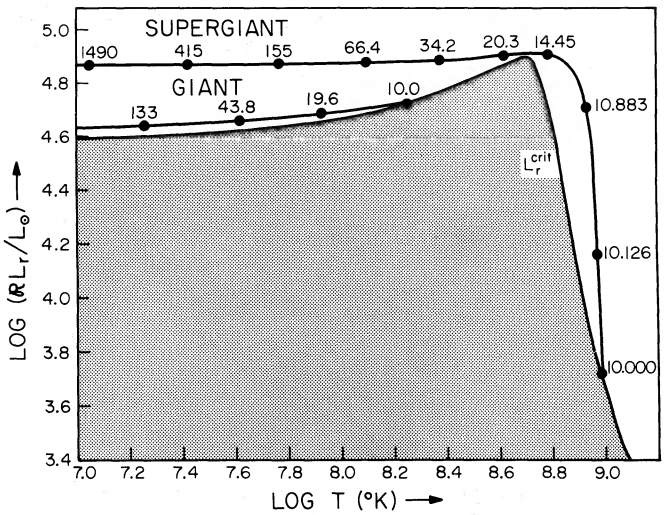

FIG. 4.—Local luminosity L_r and critical luminosity L_r^{crit} as functions of temperature T in the inflowing envelopes of the 5 $M_\odot$ giant model of Table 1, and the 12 $M_\odot$ supergiant model of Table 2. We actually plot vertically L_r and L_r^{crit} multiplied by the red-shift factor $\mathcal{R}$ because the product $\mathcal{R}L_r^{crit}$ is very nearly a function of temperature only and is therefore the same for all models with the same core masses (cf. eqs. [5.1], [5.2]). The L_r curves are parametrized by radius r in kilometers. The knee (r = 10.0 km) occurs where L_r goes subcritical.

(eq. 2.32). The product $\mathcal{R}L_r^{crit}$ is plotted, as a function of temperature T for $X_{ph} = 0.70$, $M_{tc} = 1\ M_\odot$, and $\rho \sim (10\ \mathrm{g\ cm^{-3}})(T/10^9\ \mathrm{K})^3$, in Figure 4. (The dependence on ρ, which is exceedingly weak and can be ignored, enters through the ratio n_+/n_e of pairs to ionization electrons; see the Appendix.) At low temperatures ($T \lesssim 10^7$ K), $\mathcal{R}L_r^{crit}$ is constant; but at $T > 10^7$ K the Klein-Nishina corrections $G(T)$ begin to reduce the electron-scattering opacity, and thereby increase $\mathcal{R}L_r^{crit}$. At $\log T \approx 8.70$, when $\mathcal{R}L_r^{crit}$ has increased by a factor 2.0, electron-positron pairs turn on, increasing the number of photon scatterers, thereby increasing κ_{es}, and thence decreasing $\mathcal{R}L_r^{crit}$. The turn-on of pairs with increasing T is so sharp above $\log T = 8.70$ that $\mathcal{R}L_r^{crit}$ plummets dramatically (see Fig. 4).

In the envelopes of our models the local luminosity L_r is everywhere supercritical (see § IV*a*). Moving inward through the envelope, one reaches the knee (termination of convection) immediately after L_r goes subcritical. Figure 4 shows two $L_r(T)$ curves: one for the interior of a giant model, the other for the interior of a supergiant. The difference between the two is obvious: The giant goes subcritical, with increasing T, before the peak of $\mathcal{R}L_r^{crit}$ is reached. The supergiant has such a high luminosity that it passes over the peak; but shortly thereafter hydrogen burning turns on, driving L_r down through the now plummeting L_r^{crit} curve. The hydrogen burning has to generate a very large luminosity ($L_{nuc} \approx L$) in order for L_r to catch up with the rapid plummet of L_r^{crit}.

The sharpness of the pair turn-on at $\log T = 8.70$ (the sharpness of the peak in L_r^{crit}) is responsible for the mass gap between our giant and supergiant models. For a model in the mass gap one can choose a total luminosity L such that L_r goes subcritical very slightly before the L_r^{crit} peak (giant-type structure); but such a choice always leads to a knee radius r_K larger than the desired core radius R_c—and thus to no viable model. If one chooses L slightly larger, so that L_r skims over the L_r^{crit} peak and somewhat later plummets due to hydrogen burning (supergiant-type structure), one obtains a knee radius r_K smaller than R_c—and again no viable model. No choice of L can produce the desired knee radius.

Unfortunately, the above discussion is based on an inadequate treatment of hydrogen burning: Our detailed models utilized a CNO-cycle burning rate appropriate to the temperatures of normal stars ($T \sim$ [2 to 10] $\times 10^7$ K), whereas in our supergiants the hydrogen-burning shell has $T \approx 10^{8.9}$ K. The "hot CNO–Ne cycle" burning rates of Audouze, Truran, and Zimmerman (1973) would be more appropriate. However, even they would be extremely inadequate: Some of the crucial β-decays involved in the hot CNO–Ne cycle have lifetimes of $\sim$1 to 100 seconds, whereas convection circulates matter into and back out of our hydrogen-burning shell in a time $\Delta t \sim 0.01$ s (cf. Table 2). For this reason we expect hydrogen burning to proceed in the following very unconventional manner: Convection circulates unburned matter into the hydrogen-burning shell, where all strong interactions go to completion almost instantaneously ($\Delta t \ll 0.01$ s). The reaction chains then get hung up waiting for β-decays to proceed. After $\sim$0.01 s the β-hung-up matter gets swept back up to larger radii (lower temperatures), where it convectively random-walks from place to place, while undergoing β-decay. Sometime later, after the β-decay is partially or fully complete, the matter random-walks its way back into the hydrogen-burning shell, where its strong interactions proceed once again.

In a subsequent paper we hope to analyze supergiant hydrogen burning from this point of view. We presume that

the reaction products will include very peculiar relative abundances of various catalyst isotopes, and that these may provide an observational handle for stars with neutron cores (see § I*c*).

It is quite possible that an improved treatment of hydrogen burning will change the hydrogen-shell structure of our supergiants substantially, and will destroy the mass gap between giants and supergiants.

VI. STABILITY OF OUR MODELS

We have worried about five possible instabilities in our stellar models:

Dynamical instability of the envelope, caused by the low adiabatic index ($\Gamma_1 < 4/3$) in the regions of hydrogen and helium ionization, where much of the envelope mass resides. The situation here is similar to that in red supergiants with degenerate white-dwarf cores (cf. Paczynski and Ziółkowski 1968), since the envelopes there and here are nearly identical. In such envelopes the thermal and hydrodynamical time scales are comparable, so energy transport has a strong influence on the time development of any instability. We have analyzed the stability of our envelopes ignoring energy transport (stability against linearized *adiabatic*, radial perturbations); see last column of Tables 3 and 4. For envelope masses $M_{\rm env} \lesssim 2\ M_\odot$ our envelopes are adiabatically unstable; for $M_{\rm env} > 2\ M_\odot$, they are adiabatically stable. This result suggests (see, e.g., Keeley 1970*a*,*b*;) that a more correct, nonadiabatic analysis may reveal either pulsational or disruptive instabilities for our least massive envelopes; but that our most massive envelopes *might* be stable against all perturbations, except convective ones.

Thermal instability of the shell sources. Consider a nonconvective shell source with average luminosity and temperature $\bar{L}_r$ and $\bar{T}$, and with luminosity and temperature drop across itself of ΔL_r and ΔT. A crude analysis (simple generalization of page 857 of Schwarzschild and Härm 1965) shows that an average temperature rise of δT inside the shell produces the following rate of increase of the shell's internal energy:

$$\frac{dE_{\rm internal}}{dt} = (\Delta L_r)\left[\nu - 8\,\frac{\bar{L}_r}{\Delta L_r}\,\frac{\bar{T}}{\Delta T}\right]\frac{\delta T}{\bar{T}}\,. \tag{6.1}$$

Here ν is the temperature exponent of the nuclear-burning rate, $\epsilon \propto T^\nu$. The nonconvective halos of our models are extremely isothermal—so isothermal that $8(\bar{L}_r/\Delta L_r)(\bar{T}/\Delta T)$ has values of $\sim$30 to 40 for the giant model of Table 1, and $\gtrsim$1000 for the supergiant of Table 2. This is sufficiently large compared to ν that our nonconvective halos are probably stable against thermal runaway (positive δT sets up a heat flow out of the shell which exceeds the increased nuclear burning). Even if the nonconvective shell sources turn out to be unstable, their very small contribution to the star's total luminosity, and their location deep below the envelope, and the very short time scale of the instability will probably prevent the instability from producing observable effects at the photosphere.

In our supergiant models the convective hydrogen shell source should be protected from thermal runaway by the β-decay hang-up discussed in § V. On the other hand, the convective hydrogen burning described in § V might proceed in a series of local flashes rather than as a smooth energy flow. Even if this is the case, the time scale of the flashes will be so short ($\Delta t \ll 1$ s) that their effects presumably will be smoothed out in the overlying envelope.

Instability of the region of gravitational energy release ($\rho_K < \rho \lesssim 10\,\rho_K$). We do not now have any insight into the stability of this region. Any adequate analysis would have to take account of convective overshoot.

Runaway neutrino losses, accompanied by an ever-increasing rate of envelope contraction. The computations of Zel'dovich, Ivanova, and Nadyozhin (1972) suggest that such an instability may occur in models with halo temperatures much higher than ours—if such models can exist. However, our low halo temperatures ($T \lesssim 1 \times 10^9$ K) keep the middle-region neutrino losses small ($\ll 1\ L_\odot$) and presumably will prevent them from running away. Because of thermal decoupling (§ II*b*), neutrino losses in the core cannot produce an instability in the overlying halo and envelope.

Instability of the mass inflow pattern. Bisnovatyi-Kogan (private communication) has argued that the inflowing envelope, halo, and outer core may be unstable against perturbations which break the radial constancy of $\dot{M}$. A specific example of such an instability is the possibility (Cameron, private communication) that at densities $\sim 3 \times 10^8$ to $\sim 10^{14}$ g cm^{-3} rapid pycnonuclear reactions and electron capture, followed by intensive neutrino-antineutrino emission, might produce a rapid shrinkage of the outer core. We doubt that such instabilities exist, but we have no proof.

A Henyey-type evolutionary calculation would be a powerful tool to use in testing for the above instabilities and others.

VII. EVOLUTION OF OUR MODELS

We saw in § IV*d* that stars with neutron cores can occupy only an extremely narrow strip in the H-R diagram, sitting precisely on the edge of the Hayashi forbidden region. The boundaries of this strip can be found with good accuracy by static-envelope integrations; see § IV*d* and Figure 3.

Take a star with a neutron core and a given total mass M_t, and assume that it does not undergo any violent instabilities during the time required for its core mass M_{tc} to grow significantly. Such a star should evolve through a sequence of quasi-equilibrium states of the type discussed in this paper. Restrict attention to giant-type stars, for which the envelope does not evolve chemically. Then the evolution of the surface features, L and $T_{\rm ph}$, can be read off a static-envelope H-R diagram such as Figure 3, without any reference to the structure of the inflowing envelope

or halo. As M_{tc} increases, L and T_{ph} must move up the narrow allowed strip (strip with $T_{o-m} \sim 10^6$). The evolution will terminate by collapse of the core to form a black hole when M_{tc} reaches the Oppenheimer-Volkoff limit (maximum mass of neutron star) $M_{OV} \sim 1.5$ or $2\ M_\odot$.

To verify for a given star that giant-type evolution (unchanging envelope abundances) really is reasonable, and to learn the details of evolution of the star's deep interior, one must construct a sequence of evolutionary models for the entire stellar envelope and halo. One could do so using a Henyey-type code. However, we think this is not necessary. Assuming that our models are stable, Henyey evolution would have to reproduce the unique sequence of models which we obtain by our methods holding the star's total rest mass M fixed and increasing its core mass M_c from model to model. Such a sequence would be nearly the same as the one shown in Table 4 with fixed total mass M_t and increasing M_{tc}.

The evolutionary sequence in Table 4 is for a star with total mass $M_t = 5\ M_\odot$, with envelope abundances $X_{ph} = 0.70$, $Y_{ph} = 0.27$, $C_{ph} = 0$, and with core mass increasing from $0.40\ M_\odot$ initially to a final, Oppenheimer-Volkoff limit of $1.625\ M_\odot$. The core radius-mass relation $R_c(M_{tc})$ is that of Malone, Johnson, and Bethe (1975, their model V-H). In our models we were satisfied with reproducing the desired $R_c(M_{tc})$ to within about 1%. All models in our evolutionary sequence (Table 4) have giant-type structures. As one might expect, as the core mass grows and the acceleration of gravity at the core edge increases, the thickness of the halo decreases (cf. § IV*b*). The total time required for evolution from $M_{tc} = 0.4\ M_\odot$ to the point of core collapse, $M_{tc} = 1.625\ M_\odot$, is

$$\Delta t = \int \dot{M}^{-1} dM_c = \int \dot{M}^{-1} \mathscr{R}_c^{-1} dM_{tc} \approx 7.4 \times 10^7 \text{ years}. \tag{7.1}$$

The evolution of a supergiant is more complex than that of a giant; it is driven not only by core growth, but also by chemical evolution of the envelope. The rate at which envelope hydrogen is burned by the shell sources of our models to form envelope helium is typically ~ 500 times greater than the rate at which envelope matter flows into the core; see Table 3. To burn all of its envelope hydrogen, a supergiant of $12\ M_\odot$ requires $\sim 1.1 \times 10^7$ years, and a supergiant of $25\ M_\odot$ requires $\sim 1.4 \times 10^7$ years. For comparison, the time required for the core rest mass to increase $1\ M_\odot$ is $\sim 6 \times 10^8$ years in the first case and $\sim 7 \times 10^8$ years in the second. These estimates may be in serious error because they are based on our inadequate treatment of the hydrogen burning (§ V) and on models (Table 3) of one chemical composition only. We have not yet attempted to construct supergiant models with hydrogen-deficient envelopes.

VIII. CONCLUSION

We regard this paper as merely a first rough overview of stellar models with neutron cores. This overview has uncovered a large number of problems which must be resolved before the theory will be in satisfactory shape. At present we are pursuing only three of these problems vigorously: the details of nuclear burning and nucleosynthesis in supergiant models (§ V), the resulting chemical evolution (§ VII), and the possibility of discovering such stars by observation of peculiar photospheric abundances (§ I*c*).

Other problems that require study are these: (i) The stability of our models, with emphasis on the five possible instabilities described in § VI. (ii) A search for models with very different structures from those exhibited in this paper—e.g., models with large neutrino losses supplied by large mass inflow rates (cf. § IV*a* and § VI) and models in which profuse electron-positron pairs replace large L_r as the source of reasonable scale heights above the halo (§ IV*a*). (iii) The effect of convective overshoot on the structures of our giant models (§ IV*b*). (iv) The effect of magnetic fields in reducing the opacity at densities $10^6 \lesssim \rho \lesssim 3 \times 10^{11}$ and thereby permitting significant heat transfer between core and halo (§ II*b*).

All of the above problems seem somewhat tractable. Less tractable, but obviously very important, is the issue of how such stars might form in nature (Ostriker and Paczynski 1975).

We are deeply indebted to Bohdan Paczynski for suggesting this research problem, for many helpful discussions during its execution, and for making available to us his envelope integration program GOB and the neutrino-loss and C+C subroutines for our middle-region integrations. We also gratefully acknowledge valuable discussions with Yevgeny Bisnovatyi-Kogan, Wojciech Dziembowski, Douglas Eardley, Douglas Keeley, Jeremiah P. Ostriker, and Martin Schwarzschild, as well as valuable assistance in numerical work from Barbara Zimmerman.

APPENDIX

ELECTRON-POSITRON PAIRS IN THE NONRELATIVISTIC, NONDEGENERATE APPROXIMATION

In thermodynamic equilibrium at temperature T, the number density of electrons "$-$" and positrons "$+$" in phase space is

$$\mathscr{N}_\mp \equiv \frac{dN_\mp}{d^3x d^3p} = \frac{2}{h^3} \frac{1}{1 + \exp\left[(p_0 \mp \mu)/kT\right]}, \tag{A1}$$

where μ is the chemical potential, $p_0 \equiv (m^2 + p^2)^{1/2}$ is the total mass-energy of a particle, p is the magnitude of the spatial part of its 4-momentum, m is the electron rest mass, k is Boltzmann's constant, and we set the speed of light equal to unity. Here and below, equations containing double signs ($\mp$ or $\pm$) are valid for electrons (including ionization electrons and pair electrons) with the upper sign and for positrons with the lower sign. The number densities in physical space $n_\mp$, the pressure $P_\mp$, and the energy densities including rest mass are

$$n_\mp = \int \mathcal{N}_\mp d^3p\,, \qquad P_\mp = \tfrac{1}{3}\int (p^2/p_0)\mathcal{N}_\mp d^3p\,, \qquad \epsilon_\mp = \int p_0 \mathcal{N}_\mp d^3p\,, \tag{A2}$$

where $d^3p = 4\pi p^2 dp$.

We assume that the number of electrons exceeds the number of positrons, so $\mu > 0$; and we specialize to the nonrelativistic, nondegenerate regime:

$$\mu > 0\,, \qquad m/kT \gg 1\,, \qquad (m - \mu)/kT \gg 1\,. \tag{A3}$$

In this regime relativistic particles make negligible contributions to $n_\mp$, $P_\mp$, and $\Pi_\mp$; consequently, we can set $p^2/2m \ll m$, and use

$$p_0 = m + p^2/2m\,. \tag{A4}$$

Assumptions (A3) then allow us to write

$$\mathcal{N}_\mp = \frac{2}{h^3}\exp\left(-\frac{p^2}{2mkT}\right)\exp\left(\frac{\pm\mu - m}{kT}\right). \tag{A5}$$

By inserting expressions (A4) and (A5) into (A2) and integrating, we obtain the following results: (i) The electron and positron pressures and energy densities are given by the usual nonrelativistic expressions

$$P_\mp = n_\mp kT\,, \qquad \epsilon_\mp = n_\mp(m + \tfrac{3}{2}kT)\,. \tag{A6a}$$

(ii) The number densities of electrons and positrons are

$$n_\mp = (2/h^3)(2\pi mkT)^{3/2}\exp\left[(\pm\mu - m)/kT\right]. \tag{A6b}$$

The number density of ionization electrons n_e is the difference between n_- and n_+—and is also equal to $\rho/m_{\rm H}\mu_e$, where μ_e is the mean molecular weight per electron:

$$\rho/m_{\rm H}\mu_e = n_e = n_- - n_+ = (2/h^3)(2\pi mkT)^{3/2}\, e^{-m/kT}[e^{\mu/kT} - e^{-\mu/kT}]\,. \tag{A7}$$

Let us introduce the parameter

$$y \equiv \frac{h^3 n_e}{4(2\pi mkT)^{3/2}}\, e^{m/kT} = \left(\frac{\rho_6/\mu_e}{7.37}\right)\left(\frac{5.93}{T_9}\right)^{3/2}\exp\left(\frac{5.93}{T_9}\right), \tag{A8}$$

where ρ_6 is density in units of 10^6 g cm^{-3} and T_9 is temperature in units of 10^9 K. Then by solving equation (A7) for $e^{\mu/kT}$ we obtain

$$e^{\mu/kT} = y + (y^2 + 1)^{1/2}\,; \tag{A9}$$

and by combining with (A6b) we obtain for the ratio of number of electron-positron pairs to number of ionization electrons

$$\frac{n_+}{n_e} = \frac{n_- - n_e}{n_e} = \frac{1}{2y[y + (1 + y^2)^{1/2}]}\,. \tag{A10}$$

Equation (A6a) then shows that the ionization electrons make the usual contribution to the pressure and energy density, while the pairs make the contribution (in cgs units)

$$P_{\rm pair} = 2n_+ kT = \frac{(\rho/\mu_e m_{\rm H})kT}{y[y + (1 + y^2)^{1/2}]} \tag{A11a}$$

$$\rho\Pi_{\rm pair} = 2n_+(mc^2 + \tfrac{3}{2}kT) = \frac{(\rho/\mu_e m_{\rm H})(mc^2 + \tfrac{3}{2}kT)}{y[y + (1 + y^2)^{1/2}]}\,. \tag{A11b}$$

The temperature-density regime in which the above expressions are valid can be deduced by combining equations (A8), (A9), and (A3):

$$T_9 \ll 5.93\,, \qquad \frac{\rho_6}{3.69\mu_e} \ll \left(\frac{T_9}{5.93}\right)^{3/2}. \tag{A12}$$

The T-ρ curve along which the number of pairs equals the number of ionization electrons is given by $y = 0.354$ and is shown graphically in Figure 2. Note that when our stellar interiors cross over this curve so pairs become important, they remain well within the realm of validity of our approximations, equations (A12).

REFERENCES

Arnett, W. D., and Truran, J. W. 1969, *Ap. J.*, **157**, 339.
Audouze, J., Truran, J. W., and Zimmerman, B. A. 1973, *Ap. J.*, **184**, 493.
Auman, J., Jr. 1967, *Ap. J. Suppl.*, No. 127, **14**, 171.
Beaudet, G., Petrosian, V., and Salpeter, E. E. 1967, *Ap. J.*, **150**, 979.
Canuto, V. 1970, *Ap. J.*, **159**, 641.
Cox, A. N., and Stewart, J. N. 1968, *Scientific Information of the Astronomical Council, Acad. of Sci. USSR*, **15**, 1.
Cox, J. P. and Giuli, R. T. 1968, *Principles of Stellar Structure*, Vol. **1**, *Physical Principles* (New York: Gordon & Breach).
Eggleton, P., Faulkner, J., and Flannery, B. P. 1973, *Astr. Ap.*, **23**, 325.
Flowers, E., and Itoh, N. 1975, preprint, New York University.
Gamow, G. 1937, *Structure of Atomic Nuclei and Nuclear Transformations* (Oxford: Oxford University Press), pp. 237 and 238.
Joss, P. C., Salpeter, E. E., and Ostriker, J. P. 1973, *Ap. J.*, **181**, 429.
Keeley, D. A. 1970*a*, Ph.D. thesis, California Institute of Technology.
———. 1970*b*, *Ap. J.*, **161**, 643.
Landau, L. D. 1937, *Doklady Akad. Nauk USSR*, **17**, 301 [English transl. in *Nature*, **141**, 333 (1938)].
Malone, R. C., Johnson, M. B., and Bethe, H. A. 1975, *Ap. J.*, **199**, 741.
Oppenheimer, J. R., and Volkoff, G. 1939, *Phys. Rev.*, **56**, 455.
Ostriker, J. P., and Paczynski, B. 1975, private communication.
Paczynski, B. 1969, *Acta Astr.*, **19**, 1.
———. 1970*a*, *Acta Astr.*, **20**, 47.
———. 1970*b*, *Acta Astr.*, **20**, 287.
Paczynski, B., and Ziółkowski, J. 1968, *Acta Astr.*, **18**, 255.
Salpeter, E. E., and Van Horn, H. 1969, *Ap. J.*, **155**, 183.
Sampson, D. H. 1959, *Ap. J.*, **134**, 734.
Schwarzschild, M., and Härm, R. 1965, *Ap. J.*, **142**, 855.
Stothers, R., and Cheng, A. 1974, unpublished research.
Thorne, K. S. 1977, *Ap. J.*, **212**, 825.
Thorne, K. S., and Żytkow, A. N. 1975, *Ap. J.* (*Letters*), **199**, L19.
Tsuruta, S., and Cameron, A. G. W. 1966, *Canadian J. Phys.*, **44**, 1863.
Tsuruta, S., Canuto, V., Lodenquai, J., and Ruderman, M. 1972, *Ap. J.*, **176**, 739.
Zel'dovich, Ya. B., Ivanova, L. N., and Nadyozhin, D. K. 1972, *Astr. Zh.*, **49**, 253 [English transl. *Soviet Astr.—AJ*, **16**, 209 (1972)].

KIP S. THORNE: W. K. Kellogg Radiation Laboratory 106-38, California Institute of Technology, Pasadena, CA 91125

ANNA N. ŻYTKOW: Institute of Astronomy, Polish Academy of Sciences, Aleje Ujazdowskie 4, 00–478 Warsaw, Poland